Journal Pre-proof

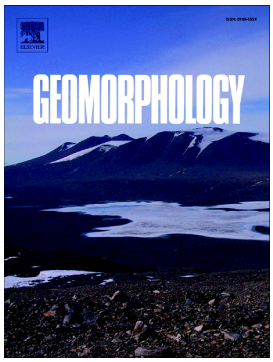

Unravelling litho-structural and tectonic influences on geomorphic and river longitudinal profile character in the Brahmani River Basin of eastern India

Aditi Roy, Priyank Pravin Patel, Anjan Sen

PII: S0169-555X(24)00526-9

DOI: https://doi.org/10.1016/j.geomorph.2024.109574

Reference: GEOMOR 109574

To appear in: *Geomorphology*

Received date: 15 June 2024

Revised date: 30 November 2024

Accepted date: 10 December 2024

Please cite this article as: A. Roy, P.P. Patel and A. Sen, Unravelling litho-structural and tectonic influences on geomorphic and river longitudinal profile character in the Brahmani River Basin of eastern India, *Geomorphology* (2024), https://doi.org/10.1016/j.geomorph.2024.109574

Unravelling litho-structural and tectonic influences on geomorphic and river longitudinal profile character in the Brahmani River Basin of eastern India

Aditi Roy[1], Priyank Pravin Patel[2], Anjan Sen[1*]

[1] Department of Geography, Delhi School of Economics, University of Delhi, New Delhi, India

[2] Department of Geography, Presidency University, Kolkata, West Bengal, India

*Corresponding author:

Anjan Sen,

Professor, Department of Geography, Delhi School of Economics, University of Delhi, New Delhi - 110007, India

Email: dr.anjansen@gmail.com, asen@geography.du.ac.in

Unravelling litho-structural and tectonic influences on geomorphic and river longitudinal profile character in the Brahmani River Basin of eastern India

Abstract

The Brahmani River basin in eastern India exhibits marked influence of tectonic and litho-structural control in its incised stream reaches, sharp changes in channel direction and the presence of numerous structural discontinuities. The combined effect of these attributes in shaping the basin geomorphology and landscape character are analysed through detailed morphometric evaluation at the sub-watershed level, overlaying lithological and geomorphic units on relevant terrain parameters extracted from Copernicus-DEM tiles and ancillary map information. Alongside this, we also analyse the longitudinal profile character of the principal stream and its main tributaries to discern knickpoints and their locations in terms of rock types and their origin, discerning that these are mostly situated in granitic and quartzite terrain and at elevations above 100 m. Stream gradient (SL) index plots show that higher values denote uplifted, tectonically affected areas, often near vertical knickpoints along fault zones in varying litho-structural units. Computed Chi (χ) plots suggest zones of river capture and drainage divide migration, with χ values decreasing from north to south across the basin and sub-watershed divides shifting towards northwest for the Lawa river, north-eastwards for the Sankh, South Koel and North Karo rivers, and towards southeast for the South Karo river. The probable paleo-surfaces and paleo-profiles of these streams is also reconstructed, based on their present longitudinal elevation and the initial uplift extents are estimated (~540 m uplift and ~45 m uplift in the upper basin and lower basin zones, respectively). The overall analysis makes it evident that most of the channel segments are not in an equilibrium phase, thus denoting the continued influence of structural and possible latter-day tectonic movements (as evidenced by recent local seismic activity), through reactivation of the crustal-scale basement faults, shear zones and mobile belts that lie astride and across the Brahmani Basin in the Eastern Ghats hills.

Keywords: morphotectonic and structural influences; basin geomorphometry; DEM-based terrain evaluation; river network and profile analysis; paleo-surface uplift and landscape evolution

1. Introduction

Drainage networks are not only a significant driving force of geomorphic change, but can also reveal the impacts of other driving forces in landscape evolution, through modifications in channel planform, geometry, gradient, and topology (Whipple and Tucker 1999; Kirby and Whipple, 2012). Bedrock channels dynamically regulate their morphology including slope, incision rates, water and sediment discharge, being influenced by the intricate interplay of basin topography, tectonic/seismic activity, climatic and litho-structural drivers, thereby influencing landscape evolution, and defining local base levels for adjacent hillslopes (Gailleton et al., 2020; Leonard., 2023).

Tectono-geomorphic activity and anthropogenic stressors significantly affect the longitudinal equilibrium of a river by creating knickpoints that modify river profiles and base levels, posing challenges in distinguishing between natural and human-induced landscape changes (Zhou et al., 2021; Chen et al., 2023). Various studies have revealed that natural/human-made dams have a significant impact in modifying the channel slope, further shaping river longitudinal profiles. (Korup et al., 2010; Zhao et al., 2019). Moreover, topographic signatures can provide insights into the geological and climatic past of a region by showcasing relict landscapes or elevated peneplains that have been shaped by paleo/previous erosion events, shedding light on landscape evolution and the impact of river shifting/capture on erosion processes (Yang et al., 2015; Yaaqoub and Essaifi, 2023). Recent studies have also documented that the reactivation of pre-existing lineaments can significantly contribute to the disequilibrium in river profiles by altering tectonic conditions, thereby affecting erosion rates and inducing drainage reorganization (Whipple et al., 2007; Mudd et al.,2014; Guha and Jain, 2020; Godin et al, 2023; Kothyari et al., 2024).

Several researchers have utilized various geomorphometric indices along with river longitudinal and swath profile analysis, stream length gradient (SL) index and knickpoint extraction methods to infer the influence of paleo or active tectonic activity, precipitation effects, litho-structural variations, differential rock resistance, regional uplifts and Holocene anthropogenic stresses on the rearrangement of drainage networks and evolution of river profiles (e.g. Divyadarshini et al., 2017; Donnaloia et al., 2019; Jaiswara et al., 2019; Boulton., 2020; Delcaillau et al., 2022; Peyerl et al., 2023; Yang et al., 2023; Yaqoub and Essaifi, 2023). Alongside these, normalized channel steepness (K_{sn}) and concavity indices are other important indicators for assessing incision and uplift rates using the slope area and integral methods, with the latter refined by the chi (χ) parameter to enhance data accuracy and address error propagation issues (Whipple, 2004; Berin and Anderson, 2007; Whittaker et al., 2007; Perron and Royden, 2013; Wang et al., 2017).

Peninsular India showcases a rich mosaic of landscapes and landforms, with diverse lithologies underlain by ancient cratonic roots, sculpted by weathering and erosion over geological time scales. While numerous studies have explored these aspects in the tectonically active Indian Himalayan region (e.g. Patel, 2013; Pathak et al., 2015; Jaiswara et al., 2020; Kothyari et al., 2020; Joshi et al., 2021; Zhou et al., 2021; Patel et al., 2022; Solanki and Gupta., 2022; Gururani et al., 2023; Negi et al., 2023; Bian et al., 2024), such research on the more stable tectonic landscape of the Indian peninsula remains rather limited (Guha and Patel., 2017; Guha and Jain., 2020; Das et al., 2022; Vidya et al., 2023). The Brahmani River basin is located within the peninsular shield and is part of the Chotanagpur Gneiss Complex and Singhbhum cratonic complex of eastern India. It traverses the Eastern Ghats ranges, draining locales on either flank of these hills. Several large dams in recent decades have significantly disrupted its natural hydrology and sediment dynamics, leading to notable geomorphometric alterations within the Brahmani River basin (Pradhan et al., 2021).

The present study initially focuses on the quantitative geomorphometric analysis of 280 sub-watersheds of Brahmani River basin to identify and isolate the driving factors for changing the basin shape

and morphology. Besides, we also identify the knickpoints, river reach gradients, tectonic signals, topographic variabilities, erosion patterns, channel incision rates and their relation with the underlying lithology, rainfall pattern and anthropogenic impoundments (dams and reservoirs), utilizing parameters related to the respective river longitudinal, swath and SL (stream length gradient) profiles. Furthermore, the standard channel steepness metric (K_{sn}) and Chi (χ) analysis have been utilised to detect the relict landscape, possible instances of river capture, channel disequilibrium and stability, where the K_{sn} fundamentally assumes that the climate is of uniform type in the whole study area. Lastly, the longitudinal profiles of the Brahmani's two primary tributaries (Sankh River and South Koel River) were reconstructed with reference to initial net surface uplift and the discerned paleo relief.

Such investigations have hitherto seldom been undertaken for the Brahmani River. Thus, this study provides significant newer and fresh perspectives into the region's landscape evolution, past uplift dynamics, river incision patterns, and possible tectonic reactivation in the relatively understudied Eastern Ghats region of the Indian peninsula. Moreover, this research contributes to understanding how geological, climatic, and tectonic/structural controls shape river basins, which has ramifications for sustainable watershed management and addressing the challenges of anthropogenic stressors.

2. Study area

The Brahmani flows through the states of Jharkhand, Odisha, and Chhattisgarh in eastern India, with a channel length of 799 km and a peak flow of 22,640 m^3/s, making it one of the largest rivers of peninsula India (CWC, 2012). Its basin covers approximately 40,000 km^2, spanning from 20°29′50″N to 23°37′2″N and 83°52′55″E to 87°1′23″E (Fig. 1). It holds a notable status among India's 14 major perennial rivers, alongside the Ganga, Brahmaputra, and Mahanadi, boasting an annual flow of 11,649 million m^3 and a storage capacity of 3953 million m^3 (Panda, 1990).

The South Koel River, which originates at an elevation of ~600 m close to Ranchi, converges with the Sankh River emanating from the Mahasamund Hills of Chhattisgarh at Vedavyas (22°14′28″N,

84°47′49″E) in Odisha. At this point, it takes the name Brahmani and traverses through Sundargarh, Keonjhar, Dhenkanal, Cuttack, and Jajpur districts. Finally, the river empties into the Bay of Bengal at Dhamra, an area known for its high susceptibility to flooding and tropical cyclones (Rai et al., 2018).

The Brahmani links the Archaean Chotanagpur Plateau province to the Holocene coastal plains of the Bay of Bengal, by cutting through the hill ranges of the Eastern Ghats. Its significant tributaries are the Sankh, South Koel, Tikra, Lawa, Samij and Karo rivers. Two significant river interventions occur on the main channel of the Brahmani River near Talcher, namely, the Rengali Dam and the Samal Barrage. The Rengali Dam (70 m), with gross and effective storage capacities of 5.15 km^3 and 3.41 km^3, respectively, has played a crucial role in modifying the river's form and processes, influencing the surrounding geomorphic unit assemblage (Mishra, 2002; CWC and NRSC, 2014). Operational since 1985, it has altered sediment transport dynamics, resulting in the river changing from a sinuous to a weakly braided channel pattern during the post-dam period (Pradhan et al., 2019, 2021). Other dams like the Mandira and Upper Sankh Dams have been constructed on the Sankh River in 1959 and 2008, respectively, while the Latratu Dam was built on the North Karo River in 1988.

2.1. Basin geological and geomorphological attributes

The study area, located within the Indian shield, is a part of the Chotanagpur mobile belt, Singhbhum mobile belt and Eastern Ghats mobile belt, and thus showcases a variety of lithological formations. These Precambrian mobile belts, indicative of proto-plate collision zones, are prime sites for rifting due to basement reactivation via crustal stretching (Daly et al., 1989; Mahadevan, 2002; Sanyal and Sengupta, 2012). This region is also an ideal example of a half-graben, viz. the Gondwana Damodar-Koel graben and is bordered by the Mahanadi graben (Mukhopadhyay et al., 2010; Choudhuri et al., 2023), forming parallel lineaments (GSI, 2012). The different lithological groups of this region attest to its complex geological history of numerous tectono-thermal events.

The Chotanagpur region underwent three significant uplift events during the Cenozoic era as a flexural reaction to the subduction of the Indian plate beneath the Himalayas (Mahadevan, 2002; Mukherjee et al., 2019), leading to the formation of various geomorphological units like the *Pat* (elevated laterite-capped surfaces) region (Eocene—Oligocene), Ranchi and Hazaribagh Plateau (Miocene), and the outer Chotanagpur Plateau (Pliocene—Pleistocene), as well as several waterfalls (Weaver, 1990; Singh and Khan; 2021). Plate convergence has induced compressional stress, causing crustal shortening and subsequent uplift in the Chotanagpur granite-gneiss terrain (Rajasekhar and Mishra, 2008; Sequeira and Bhattacharya, 2020; Mohanty, 2023), initiating basement reactivation and fault formation (Sarkar and Saha, 1977; Singh and Khan, 2021).

Geologically, the Brahmani River basin comprises of the Chotanagpur gneissic complex, Gangpur group, Singhbhum granite complex, Dalma group, Ongarbira traps, Upper Bonai group, Kolhan group, Jagannathpur group, Tamparkola formation, Bonai granite group, Lower Bonai group, Peninsular gneissic complex, Gorumahishani group, Lower Gondwana group and the Eastern Ghats gneissic complex, respectively, from north to south (Fig. 2b). Its lithological composition predominantly consists of Archaean ultrabasic and ultramafic rocks (3% of the basin area), charnockites (2%), followed by Proterozoic granite gneiss (41%), shale, slate, and phyllite (18%), mica schist (4%), sandstone and conglomerate (3%), quartzite (8%), banded iron formation (BIF) (2%), Cenozoic laterite (6%), Pleistocene compact clay (2%), and Holocene newer alluvium (9%), with minimal presence of amphibolite, epidiorite, carbonated sandstone with minor coal, limestone, basalt, leptynite, dolerite, pegmatite, and tuffaceous rocks. However, most of the Archean-Paleoproterozoic rocks are very weakly compacted and weathered in nature, except the much harder BIF which is geochemically different (Bhattacharya et al., 2007), and whose presence further indicates the region's complex climatic and tectonic history (cf. Yin et al., 2023; Bekker et al., 2010).

The basin is crisscrossed by various structural discontinuities, including folds, faults, joints, fractures, dykes, shear zones, and minor lineaments. Prominent among these are the Brahmani Fault, Rourkela lineament, Malaygiri lineament, Kerajang Fault, North Orissa Boundary Fault (NOBF), Akul

fault, Sukinda thrust, Dalma thrust, Riamal shear zone, Barakot shear zone and the extension of the Singhbhum Shear Zone (Crowe et al., 2003; Chetty, 2014; Talukdar et al. 2024) (Fig. 3b). In 1997, a temporary micro-earthquake network survey by the Geological Survey of India identified a seismically active zone located 20 km south of the Rengali Dam, with clustered epicentres near the NOBF and Brahmani River junction, indicating an active fault segment and possible asperity zone influenced by tectonic strain accumulation from current plate movements (Gupta et al., 2014; Roychowdhury, 2019). Several geothermal springs and past seismic epicentres are scattered throughout the basin (Jena et al., 2020), whose presence can feasibly lead to the surmise of a possible reactivation of the existing basement and boundary faults (Fig. 2b) (Jaiswal and Sinha, 2007; Gupta et al., 2014; Pradhan and Jena, 2016).

The basin geomorphology is characterized by a complex landscape that includes dissected hills and plateaus, incised valleys, pediment-pediplain tracts, alluvial and coastal plains and deltaic deposits and floodplains. Alongside these, anthropogeomorphic entities such as quarries and mine dumps, dams and reservoirs also exist (Fig. 2a). In terms of their origin, 66% of the basin area is covered by geomorphological features that have arisen from denudational (mainly weathering induced) processes, followed by 22% of structural formation, 7% attributed to direct fluvial action, 3% to coastal influences, and 2% resulting from anthropogenic activities.

2.2. Climatic and pedological attributes

Climatic events significantly reshape river basins by influencing sediment transport, channel networks, and geomorphic activity (East and Sankey, 2020; Pradhan et al., 2021; Chalov et al., 2023). Higher rainfall or frequent storms expand channels and increase sediment flow (Naylor et al., 2017; Khan et al., 2018; Sonam et al., 2022), causing short-term aggradation followed by incision as sediment levels stabilize (Zhou et al., 2022; Li et al., 2024). Conversely, reduced runoff (due to climatic or anthropogenic causes) or vegetation loss shrinks channel networks, slowing geomorphic changes (Das et al., 2021; Grabowski et al., 2022; Luppicchini et al., 2024). Cyclic climate variations create periodic shifts between

aggradation and degradation, with sediment peaks during wetter phases, highlighting the role of climate in basin and drainage network evolution over time, especially in the Indian context (Kale, 1999, 2002; 2003). Continued erosion can enable drainage divide migration, river capture and consequent basin shape alteration (Whipple et al., 2017; He et al., 2024), and this shall generally occur over longer geological timescales than in the short-term, unless induced by extreme hydro-meteorological events.

The mean annual temperature over the Brahmani basin is 25.7 °C, with extremes ranging from 47 °C in summer to 4°C in winter. It is situated within the sub-tropical monsoon zone, where approximately 80% of the total annual precipitation occurs during the south-west monsoon season (June to September) (Dahm et al., 2016). The northern and northeastern parts are characterized by Cwa—monsoon-influenced humid subtropical type climate, and rest of the southern portion is characterized by Aw—tropical Savanna type climate (Fig. 3a) (Köppen, 1931). This basin experiences an average yearly precipitation of 1421 mm, leading to inundation in the downstream areas (CWC, 2012). For example, the floods of 28 August, 2022 impacted 50,000 people in Kendrapara district. The river drains through sandy, loamy, and coastal alluvium, which are predominantly classified as eutric fluvisols and ferric luvisols, accompanied by scattered occurrences of eutric entisols and lithosols and the upper tracts of the basin suffer marked erosion (Majhi et al., 2021).

3. Datasets and methods

3.1. Sub-watershed morphometric and geomorphological analysis

Regional geomorphological, lithological, and geological data were obtained from the Geological Survey of India's Bhukosh portal (https://bhukosh.gsi.gov.in/Bhukosh/Public), along with toposheets at 1:50,000 scale from the Survey of India. Terrain analysis through geomorphometric methods, employing measurements and mathematical models, is essential for elucidating landscape evolution, forecasting erosion dynamics, and optimizing water resource management (Patel et al., 2021b; Mukherjee and Patel, 2022), and Digital Elevation Models (DEMs) are readily used for this purpose (Patel and Sarkar, 2010; Das

et al., 2016, 2022). The spatial arrangement of the drainage network as derived from the used DEM was validated through overlays on topographic maps, complemented by verification via field observations. The denoted Strahler stream orders varied from first to eighth. In all, 280 sub-watersheds of the Brahmani River and its eight primary tributaries– the South Koel, Sankh, Lawa, North Karo, South Karo, Samij, Tikra and Nigra– were delineated, considering 3rd to 5th order streams using the hydrology tool of ArcGIS based on 30 m resolution Copernicus DEM (COP-30) data. The COP-30 DEM was released by European Space Agency in December 2019 and has been repeatedly shown to be one of the most accurate freely available one arc-second DEM datasets presently (Guth and Geoffroy, 2021; Franks and Rengarajan, 2023; Trevisani et al., 2023; Guth et al., 2024). It has a vertical accuracy of below 4 m and Root Mean Square Error (RMSE) of 1.68 m, and has been utilized in the computation of various morphometric parameters and indices (cf. Leister-Taylor et al., 2020), as detailed in Table S1 in the Supplementary Information file for this study. These 24 geomorphometric indices (see Table S1) are direct as well as indirect indicators to assess relative landscape modifications across various tectonic/structural settings, providing insights into geomorphological dynamics (Luo et al.,2023; Smith et al., 2023). Linear parameters delineate one-dimensional attributes, while aerial aspects capture two-dimensional features, and relief aspects encompass the three-dimensional characteristics of an area (Solanki and Gupta, 2022). Earthquake data from the National Centre for Seismology, India (https://seismo.gov.in/) was used for validation of the results.

Furthermore, two important statistical analysis, Pearson's correlation coefficient and Principal Component Analysis (PCA) along with PCA-WSA (Weighted Sum Analysis) were done using SPSS and Origin Pro software to study the interrelationship among the morphometric parameters and cluster similar sub-watersheds. The PCA method uses rotated factor loading matrix to identify key morphometric parameters for ranking sub-watersheds by simplifying data complexity while maintaining reliability (cf. Ghasemlounia and Utlu, 2021).

3.2. Elevation swath profiles and local relief

Swath profile analysis, integrating elevation data with other spatial information like geological structures and precipitation, plays a crucial role in regional landscape characterization (Molin et al., 2004; Luo et al., 2023). It is also useful in linking topography with geomorphic and tectonic processes across diverse landscapes. In this paper, an ArcGIS Add-In, Swath Profiler by Perez-Pena et al. (2017), was used to generate elevation swath profiles of 10 km width on either side of the trunk stream for the Brahmani and its main tributaries. This tool directly computes swath profiles for mean, maximum, and minimum topographic elevations, as well as the first (Q1) and third quartiles (Q3), from different spatial datasets, namely DEMs and the Tropical Rainfall Measuring Mission (TRMM) precipitation datasets (cf. Bookhagen and Burbank, 2006), plotted against distance along the swath. Additionally, the tool produces the Transverse Hypsometric Integral (THi*), along with local relief measurements. Consequently, these swath profiles provide comprehensive physiographic signatures that can potentially include the locations of incised riverbeds, elevated paleo-surfaces, and the extent of regional erosion, as indicated by their range of elevation (Diercks et al., 2021). The average annual rainfall dataset for the study area was acquired from http://www.geog.ucsb.edu/~bodo/TRMM/.

3.3. Stream-length gradient index and Stream power incision model (SPIM)

The Stream-Length gradient index (SL-Index), also known as the Hack Index is a commonly used parameter to assess reach-level channel steepness and relate it with the underlying lithology/structure (e.g. Troiani et al., 2014; Piacentini et al., 2020). This was extracted by the BasinMorph tool in MATLAB 2023b, following Jaiswara et al. (2020), to assess the gradient-length relationship along the Brahmani and its eight main tributaries. This also identifies abrupt changes in the thalwegs due to probable tectonic activities, litho-structural variations, and stream power alterations (Chen et al., 2003; Patel et al., 2021a). Lower SL values are indicative of ductile and less resistant underlying rocks/substrate, while higher SL values are typically associated with hard rocks and signify tectonic deformations along with active faulting (Kirby and

Whipple, 2001; Taloor et al., 2023; Ferreira de Lima et al., 2024). SL index was calculated using the equation (Hack, 1973):

$$SL = \left(\frac{\Delta H}{\Delta L}\right) \times L \qquad \text{(Eq. 1)}$$

where, ΔH/ΔL represents channel gradient or slope of the specific reach, in which ΔH is the elevation change along the reach, ΔL is the length of the channel reach and L stands for total length of the river from the midpoint of the selected segment to the channel's highest point.

In a steady-state topography, variations in spatial trends in uplift or incision along the longitudinal profile of a river are typically assessed using the Stream Power Incision Model (SPIM), a standard quantitative method (Duvall et al., 2004; Mudd et al., 2018; Mitchell and Yanites, 2021). The Normalized Channel Steepness (K_{sn}) Index is one of the most commonly used proxies, helping identify the spatial variations in bedrock uplift (U) or incision rates (E) over time (t) along channel profiles due to climatic or tectonic perturbations (Howard and Kirby, 1983; Whipple and Tucker, 1999; Wobus et al., 2006; Dibiase and Whipple, 2011). It is expressed as:

$$E = KA^m S^n \qquad \text{(Eq. 2)}$$

where, K denotes the erodibility coefficient, S is the stream gradient, A is drainage area, and 'm' and 'n' represent positive constants. Factoring in the uplift occurring in an area, Eq. 2 can be revised as (Zaprowski et al., 2005):

$$\frac{dz}{dt} = U\,(t) - E = U - KA^m S^n \qquad \text{(Eq. 3)}$$

In bedrock channels, river profiles typically achieve equilibrium by adapting to changes in upstream discharge and sediment load (Sklar and Dietrich, 2006). This leads to graded profiles being characterized by a power-law relationship between the channel slope or stream gradient (S) and the upstream drainage area (A), which controls its hillslope erosion potential (Jansen et al., 2010), and serves as an indicator of probable tectonic processes (Gilbert,1877; Flint,1974; Whipple and Tucker, 1999; Kirby and Whipple, 2001; Whipple, 2012).

$$\frac{dz}{dt} = U(x,t) - K(x,t)\, A(x,t)^m\, S(x,t)^n \qquad \text{(Eq. 4)}$$

Such a bedrock river is typically considered to be graded or in a steady state (dz/dt = 0), when its profile is adjusted such that the flow velocity is sufficient to transport the sediment load from upstream, maintaining a balance (Mackin, 1948; Schwanghart and Scherler, 2014).

$$S = \quad (U/K)^{1/n}\, A^{-(\frac{m}{n})} \qquad \text{(Eq. 5)}$$

here, θ [θ = m/n; where, m and n denote positive constants] stands for the concavity index. The concavity index (θ) and the normalized channel steepness index (K_{sn}) can be determined through linear regression analysis between the channel slope and the drainage area, presented on a logarithmic scale (Wobus et al., 2006; Kirby and Whipple, 2012).

Three fluvial erosion models: detachment-limited, transport-limited, and hybrid, have been suggested (Yanites, 2018), with detachment-limited models emphasizing the impact of channel substrate strength and base-level changes on steady-state river gradients in bedrock rivers (Tucker and Whipple, 2002; Bishop and Goldrick, 2010). An initial method was proposed by Sklar and Dietrich (1998) that calculates a reference slope (S) considering a constant reference upstream drainage area (A) to demonstrate gradient comparisons among streams of similar length, though this approach is less effective for comparing rivers of varying lengths:

$$S = K_s\, A^{-\theta} \qquad \text{(Eq. 6)}$$

where, Ks is the channel steepness index, θ is the concavity index (Flint, 1974). Later, another method assumes that the concavity index (θ) value should range from 0.4 to 0.6 in a steady-state channel (Tucker and Whipple, 2002). However, typically a θ^{ref} is particularly effective in correlating and comparing channel steepness and stream profiles across various basin sizes by determining the normalized steepness index (K_{sn}) (Wobus et al., 2006; Perron and Royden, 2013) as:

$$S = K_{sn}\, A^{-\theta ref} \qquad \text{(Eq. 7)}$$

It is also important to note that minor uncertainties in θ can result in considerable fluctuations in the K_{sn} value. For this study, the stream network was delineated using a minimum drainage area of 5 km² and reference concavity index (θ^{ref}) was calculated using the 'mnoptim' function in TopoToolbox and MATLAB, following Schwanghart et al., (2021) and Gailleton et al. (2022).

3.4. Knickpoint identification

As per the stream power model, river long profiles are anticipated to resemble a concave-up form in steady-state or equilibrium condition, whereas knickpoints are localized convex segments, and serve as geomorphic markers (cf. Keller and Pinter, 2002; Bull, 2007; Burbank and Anderson, 2011) for assessing the impact of litho-structural elements, tectonics, climate, and human activities on fluvial processes and river morphology (Crosby and Whipple, 2006; Phillips et al., 2010; Lima and Binda, 2013). Typically, knickpoints form due to base level changes, shifting the river from one equilibrium state to another (Wang et al., 2017; Ahmed et al., 2018), causing variations in channel steepness (ks) or the normalized channel steepness index (K_{sn}), and leading to non-equilibrium states when uplift does not correlate with erosion rates (Haviv et al., 2010; Kirby and Whipple, 2012; Neely et al., 2017). Thus knickpoints, primarily categorized into vertical-step and slope-break types, usually reflect the geological (litho-structural or tectonic) dynamics of a region (Haviv et al., 2010; Brocard et al., 2016; Gailleton et al., 2019). Vertical-step knickpoints are stationary and linked to different rock competencies, while slope-break knickpoints are mobile and influenced by environmental factors like faults/thrusts, uplift/incision, base level change (local/global/temporary), or water and sediment discharge variations, and show increasing steepness index (K_{sn}) downstream (Kirby and Whipple, 2012; Boulton, 2020; Hergarten, 2021; Wang et al., 2022). To determine the influence of lithological or structural or anthropogenic factors (i.e., dams and reservoirs) on knickpoints, such locations are verified through geological maps, satellite imagery, and field investigations, alongside employing slope-area plots to differentiate between break-in-slope knickpoints indicative of incision or uplift, and vertical-step knickpoints typically caused by lithological differences or

human activity (Hinze et al., 1998; Brocard, 2003; Haviv et al., 2010). Furthermore, knickpoints are identified as lithological, structural, or anthropogenic based on their proximity to lithological boundaries, tectonic structural lineaments or human-made structures (Zhou et al., 2021; Sorrentino et al., 2023). In this paper, knickpoints were identified using the 'knickpointfinder' function in TopoToolbox 2.4 embedded in MATLAB (Schwanghart and Scherler, 2017), a geometric method that compares actual stream profiles with theoretical ones based on the stream-power law. For this, to accurately identify knickpoints and avoid noises from DEM artefacts, we used the Constrained Regularized Smoothing (CRS) technique (Schwanghart and Scherler, 2017), which compares the differences between upstream maxima and downstream minima, to set a minimum elevation threshold of 30 m. Given that the vertical accuracy of the GLO-30 DEM is ±4 m, the above elevation threshold considered is far in excess of this, even factoring in induced local additional height changes that may occur due to any tall canopy cover (as the GLO-30 is a DSM product). Thus, we could feasibly assert that a ≥30 m drop along a river's profile would most likely reflect a knickpoint. Such geomorphometrically ascertained locations were subsequently verified through field surveys and via overlays of lithological, structural and geomorphological data.

3.5. River longitudinal profiles and Chi (χ)-gradient

Longitudinal profile evolution models typically depict older rivers as having more concave profiles, indicating a state closer to dynamic equilibrium, yet the degree of concavity is influenced by factors such as the discharge, sediment load and its grain size distribution (Burbank and Pinter, 1999; Phillips et al., 2010; Hergarten, 2021). Chi (χ) plots can reveal the disequilibrium that occurs due to river capture, and also provide information about relict landscapes and drainage divide stability (Willett et al., 2014; Jancewicz et al., 2022). As χ analysis uses elevation data directly, there are ess errors expected in its computation and the contribution of the tributaries to the overall channel steepness can also be ascertained (Smith et al., 2022). In order to prepare the χ-elevation plots (χ-z), initially we calculated the best-fit theta reference concavity (θ_{ref}) values from the terrain data (i.e. DEM-derived) to determine if the landscape is

in equilibrium (steady state) or disequilibrium by evaluating reach wise convex-concave deviations from the equilibrium line. We also used the standard value of $\theta = 0.45$ to comparatively analyse these values with that of other rivers (cf. Boulton et al., 2014; Clubb et al., 2023; Yao et al. 2024).

In river systems, steady state equilibrium is achieved when all tributaries joining the main river share equal elevation and χ values, while variations in elevation and χ values among tributaries indicate the migration of drainage divides from regions with lower to higher χ values (Giachetta and Willett, 2018a, 2018b; Gururani et al., 2023), and χ values typically increase with the increase in the distance from a river outlet (cf. Giachetta and Willett, 2018b; Joshi et al., 2021; Gemignani et al., 2022). Thus, as per the river capture model, areas with higher elevations and low χ values are indicative of zones of drainage gains having more erosive channels, while regions with lower elevations that display high χ values are typically associated with drainage area loss and lower erosion rate (Fan et al., 2018; Jaiswara et al., 2019; Wang et al., 2022; Kashyap et al., 2024) and watershed divide migration (Jancewicz et al., 2022). Furthermore, the aggressor or capturing river will move towards lower χ values above the equilibrium line with a comparatively higher erosion rate along with the tributaries (Kirby and Whipple., 2012, Willett et al., 2014). Consequently, the victim river will be shifted towards the right side below the equilibrium line and will be experiencing low erosion rate. However, variations in the slope-gradient of a χ-plot may also result from increased uplift rates or the presence of less easily eroded rock (Gailleton et al., 2021; Smith et al., 2022). The χ-plot for each river network within the drainage basins was determined using the 'chiplot' function in TopoToolbox 2.4, generating a linear regression on χ-elevation data to identify the best-fit optimal basin concavity and steepness indexes (Perron and Royden., 2013; Schwanghart and Scherler., 2014). Also, the reference concavity index (θ^{ref}) was calculated using the "mnoptimvar" algorithm in TopoToolbox to minimize the chi-disorder.

Being an integral method, the χ metric integrates the drainage area along the river channel network from a base level up to a specific location. This is used to analyse river long profiles and identify knickpoints

by plotting the elevation against χ, highlighting the channel network dynamics, normalized by a reference drainage area (Royden et al., 2000; Perron and Royden., 2013; Willett et al., 2014; Sorrentino et al., 2023).

$$z(x) = (z_b + \frac{U}{KA_0^m})^{1/n}\, x \qquad \text{(Eq. 9)}$$

where, z is elevation and z_b represents the base level elevation. The longitudinal coordinate χ is equal to:

$$\chi = \int_{xb}^{x} (\frac{A_0^{m/n}}{A(x)^{m/n}})\, dx \qquad \text{(Eq. 10)}$$

where, x represents upstream location, x_b denotes base level, m and n are constants and m/n ratio = θ (concavity), A_0 denotes arbitrary reference drainage area, χ represents strength of erosivity and tectonic force, equivalent to K_{sn}. As per the stream-power model, under near steady-state conditions, the χ plot of a river will exhibit a linear trend with a uniform slope (Royden and Perron, 2013; Lague, 2014; Harel et al., 2016; Mitchell and Yanites, 2019).

3.6. Reconstruction of paleo river profile

Relict landscapes can be used as passive markers for the vertical movement of the Earth's crust, allowing the inference of characteristics related to the paleo relief (Clark et al., 2005; Li et al., 2021; Kaveh-Firouz et al., 2023). The equilibrium paleo river profiles of the trunk channel of the Sankh and South Koel, the two main tributaries of the Brahmani River, were reconstructed by considering the paleo base level through S-A analysis and χ analysis, using parameters such as concavity (θ) and channel steepness (K_{sn}), alongside the local channel slope (S) and drainage area (A) analysis, to identify probable relict landscapes above a significant knickpoint (cf. Clark et al., 2005; Kirby and Whipple, 2012; Gallen et al.,2013; Wang et al., 2017; Wang et al., 2017; Jaiswara et al., 2019; 2022; Li et al., 2021). Subsequently, the paleo-reliefs of the downstream reaches were reconstructed by measuring these key parameters obtained from the upper relict reach to the recent/present outlet location. Furthermore, the respective elevation difference between the paleo river profiles and their recent outlets provides a likely minimum estimation of both the total uplift

and the incision amounts due to headward migration of the upstream knickpoints (Whipple and Tucker, 1999; Whipple, 2001; Li et al., 2021; Wang et al., 2022; Rohrmann et al., 2023; Kaveh-Firouz et al., 2024).

Separately, we conducted a detailed field survey to quantitatively investigate rock strength using a rebound RockSchmidt hammer, further isolating the influence of different lithologies, based on their classification by Goudie (2006) (Table S3 in the Supplementary Information file). RockSchmidt rebound values (R) range from 1 to 100, with the lowest values indicating the weakest rock types and the highest values indicating the strongest (Goudie, 2006; Mol, 2014). The lithological unites were grouped into the same lithological units as represented in the K_{sn} and SL maps for better understanding. The strongest lithology, BIF that has a 'R' value of >40, categorized as 'Moderately strong'. Furthermore, several structural deformations and geomorphological features across the Brahmani River Basin, including major knickpoints associated with waterfalls and dams, have been ground-truth verified.

4. Results

4.1. Basin linear attributes

Stream segments within the study area were categorized into eight classes based on Strahler's (1952) method (see Supplementary Fig. S1k in the Supplementary Information file)**.** Only the 3rd, 4th and 5th order streams joining the main channel of the Brahmani River (8th order) and its major 6th and 7th order tributaries such as Lawa, Sankh, South Koel, North Karo, South Karo, Kurarhi, Tikera, Nigra, were considered to demarcate the 280 sub-watersheds (SW) (Fig. 4), as these cover almost the entire basin.

The highest total number of streams (N_u= 1063) and total length of streams (L_u= 1304 km) are reported from the sw-93 (5th order) and sw-179 (5th order) basins (Fig. 4a). The bifurcation ratio (R_b) parameter aids in interpreting inferring flood risk and litho-structural control. Notably, low (<3.0) and high (>5.0) basin-mean bifurcation ratio (R_{bm}) values indicate less and more structural control, respectively, and such deformation is likely due to past tectonic activities or existent structural control in the study area. For instance, the sub-watersheds adjacent to the Dalma and Sukinda thrusts display higher R_{bm} values.

4.2. Basin areal attributes

Areal parameters, such as drainage density (Dd), drainage texture (Dt), constant channel maintenance (CCM), infiltration number (If), length of overland flow (Lg) and stream frequency (Fs), provide insights into rock hardness and permeability, relief and runoff character (Fig. 4 and Fig. S1). As the stream order increases from 3rd to 5th, the sub-watersheds show a corresponding rise in Dd from 1.3 to 1.41 km/km² and refinement (coarse to fine) in Dt from an average of 0.711 to 2.72, indicating a shift towards denser networks, which may indicate more impermeable terrain or friable topsoil, higher relief and increased potential for runoff and erosion. Generally, higher infiltration capacity leads to reduced runoff due to the inverse relationship between If and Lg, while increased precipitation above the infiltration capacity would induce greater overland flow. For instance, in the case of sw-275, the highest Lg (1.272) and CCM (2.543) are observed, which correspond to the lowest If (0.021) and Fs (0.054).

Basin shapes can be categorized as elongated or circular based on parameters like Circulatory Ratio (Rc), Compactness Coefficient (Cc), Elongation Ratio (Re), and Form Factor (Ff). These indices collectively describe the shape, drainage efficiency, and hydrological response of a watershed, as influenced by its topography, geology, and extent of the drainage network. The 3rd order sub-watersheds (sw-46, sw-70) primarily situated in the upper Brahmani basin with higher Ff (>0.50) situated within Paleo-Proterozoic terrains of lower porosity granite-gneiss, correspond well with higher Re (>0.80) suggesting more elongated shapes. In contrast, the lowest Ff (0.20) and Re (0.53) both are obtained from sw-261 (5th order), near the downstream reach of the basin. Interestingly, the highest Circulatory Ratio (Rc) and the lowest Compactness Coefficient (Cc) are of the upstream 3rd order sub-watersheds sw-42 and sw-44, denoting more circular shape and probable runoff peakedness, whereas both the lowest Rc and the highest Cc were observed in the downstream sub-watersheds sw-173 (5th order) and sw-275 (4th order), showing inverse relationship. The asymmetry factor can determine the tectonic tilting of drainage basins at both local and large scales. This factor is sensitive to the uplift and sinking of individual blocks and incorporates potential

differential tectonic activity directions. Approximately 54.64% (153/280) of the sub-watersheds exhibit AF values >50, thereby indicating a probable slight inclination towards the left flank of the basin.

4.3. Basin relief parameters

The basin relief greatly impacts erosion rates and the removal of material from the basin. Basin-average relief (Bh) ranges between ~1107 m (sw-250) and ~49 m (sw-1), and the highest Bh and dissection index (Dis), are both reported from the sw-250, located along the Brahmani fault and Akul fault zone. The lowest Bh is linked to low ruggedness number (0.065) in sw-1. Hypsometric integrals (HI) have been computed for the sub-watersheds in order to assess their probable landscape evolution stage. Notably, the HI is influenced by the geometry of channel networks, drainage area and lithology. Most sub-watersheds within the Brahmani basin have HI values from 0.2 - 0.5, exhibiting a mean HI value of 0.3. The north-western sub-watersheds (sw-72, sw-109, sw-124) exhibit convex curves. Higher HI values (HI>0.55) are predominantly concentrated in the north-eastern part of the Brahmani River basin, indicating more youthful or less eroded landscapes, hence suggesting an 'inequilibrium stage' (Strahler, 1952). In contrast, the south-eastern sub-watersheds (sw-272, sw-275, sw-280) present concave curves and low HI values (<0.1), reflecting a typical alluvial deltaic-floodplain region where a significant portion of the landscape is nearer to the base level.

4.4. Longitudinal and swath profiles, SL Index and SPIM

Geomorphic proxies such as topographic swath profiles, stream length gradient (SL index), steepness index (K_{sn}) and Chi (χ)-gradient profiles were analysed for the main channel of Brahmani River (8^{th} order) and its major 6^{th} and 7^{th} order trunk tributaries such as the Lawa, Sankh, South Koel, North Karo, South Karo, Kurarhi, Tikera, and Nigra. The longitudinal profiles of the selected rivers display prominent knickpoints and convex reaches in their upstream sections, suggesting differential uplift or base level change of the river bed (Fig. 5 and also Fig. S2). Further, 10 km wide topographic swath profiles were utilized to examine

the trend of topography and precipitation. Almost all the tributaries represent distinct asymmetric characteristics, except Lawa. Where the difference between the highest and lowest elevation is minimal, it indicates a low relief surface. Low relief landscapes in swath profiles of the Sankh, South Koel, North karo, Tikera and Nigra are quite prominent. A noticeable decline in the average annual precipitation is observed downstream in the swath profiles of South Karo, Kurarhi, Tikera, and Nigra. Sudden step-like breaks in the swath profiles located upstream of two major tributaries, Sankh and South Koel, correspond well with the minor shear zones in the Chotanagpur gneissic complex. The longest swath profile (~360 km) of the trunk channel of the Brahmani shows strong asymmetry in the upper and middle sections due to lithological differences and several structural controls. The Brahmani fault is responsible for the prominent structural expression proximal to the location of the Rengali dam. Significantly, middle reaches of the Brahmani and Tikera rivers are affected by a major gravity fault, being denoted through asymmetric swath profiles. Precipitation patterns indicate that peak precipitation does not always occur at higher elevations; instead, mean rainfall profiles often decrease on the leeward side. Specifically, the average annual precipitation is comparatively lower in the upper reaches (plateau section) of the Brahmani River, markedly increasing in the middle and lower reaches, specifically after the river enters the plains (<100m).

Variations in the Stream Length Gradient (SL) index reveal lithological or tectonic impacts on the slope of river segments (Kale and Shejwalkar, 2008). Generally, higher SL values are associated with uplifted areas or reaches along resistant hard rocks, while lower SL values suggest less tectonic activity and less resistant bedrock (Taloor et al., 2023) (Fig. 6 and also Fig. S3). Also, the shape of the SL curve indicates the geomorphic processes operative in the watershed (Strahler,1952). The highest spike in SL index (4770) is observed in the South Koel, which possibly indicates a tectonically perturbed region, with resistant strata. In contrast, the lowest SL value (295) is reported from the Nigra River, in its downstream section over newer Holocene alluvium, that suggests a litho-structural influence on the SL values. The estimated values of SL along the main Brahmani channel range from < 1 to 2750, with highest values situated around the vertical step knickpoint along the Brahmani fault, while moderate peaks are associated with lithological

boundaries (i.e. granitic gneiss – quartzites of Paleoproterozoic age), minor faults and shear zones, indicating strong litho-structural control on landform evolution and drainage networks.

The SPIM, combined with the normalized steepness index (K_{sn}), is generally used to assess the variability in uplift along river channels under steady-state conditions, incorporating erodibility, drainage area, and basin slope factors. A reference concavity (θ_{ref}) value of 0.45 is commonly accepted as the condition for steady state in geomorphological studies globally to minimize anomalies and make results comparable (Tucker and Whipple, 2002; Whipple, 2004). The basin averaged K_{sn} values for all the 280 sub-watersheds vary widely [lowest value 1.54 (sw-280), highest value 29.40 (sw-217)]. Among all sub-watersheds, only 11 (4%) (sw-71, sw-122, sw-131, sw-136, sw-142, sw-144, sw-217, sw-218, sw-223, sw-229, sw-231) reported K_{sn} values exceeding 25, indicating localized zones of significant channel steepness and potential tectonic perturbations. In contrast, K_{sn} values < 2 in sw-275 and sw-280 suggest relatively low channel steepness, indicative of gentler terrain or relatively stable tectonic conditions (Fig. 4h).

Channel segment-wise normalized steepness index (K_{sn}) for each individual river was computed to determine the likely spatial variation in litho-structural control (Fig. 6a). Abrupt breaks in the K_{sn} values, along with the presence of various morphotectonic markers such as fault scarps, unpaired terraces, drainage offsets and knickpoints, confirmed through field observations, indicates the influence of persistent lineaments and litho-structural boundaries (see Fig. S9-S12 in Supplementary Information). The maximum K_{sn} value of 840 $m^{0.9}$ is reported from the middle reach of the main channel of river Brahmani. Hence, there is good correspondence between local external disturbances (Rengali Dam) along with presence of the Brahmani fault and different local lithological boundaries (i.e., granite-gneiss and mica-schist of Archean-Paleoproterozoic age). Conversely, the lowest K_{sn} value of ~0 is reported from the lower deltaic alluvium plain region of the same river. Furthermore, K_{sn} values higher than 400 $m^{0.9}$ are reported from the upstream higher-altitude tributaries emanating from the plateau region, e.g. Sankh (491.96 $m^{0.9}$), South Koel (516.19 $m^{0.9}$) and North Karo (466.07 $m^{0.9}$). Interestingly, despite being an upstream tributary situated in the Chotanagpur gneissic plateau, the Lawa has the lowest peak K_{sn} value at 31.13 $m^{0.9}$. Similarly, South Karo

in the Singhbhum region also shows low peak K_{sn} at 39.19 $m^{0.9}$ (Fig. 6b). Similarly, the Tikera has high K_{sn} value in its upstream section just before crossing a major gravity fault but shows moderate K_{sn} value when flowing parallel to the same gravity fault. Our findings indicate that higher K_{sn} values are mostly associated with areas characterized by a high density of lineaments and higher average annual precipitation, both of which can in combination increase the erodibility of the substrate and erosivity of the streams.

Interestingly, higher median K_{sn} values ($\geq$ 20 $m^{0.9}$) were observed in lithologies like epidiorite (23 $m^{0.9}$), dolerite (20.6 $m^{0.9}$), charnockite (20.4 $m^{0.9}$), and ultrabasic and ultramafic rocks (20.2 $m^{0.9}$), corresponding well with the respective moderately high annual rainfall amounts of 1614 mm, 1572 mm, 1244 mm, and 1461 mm. These findings suggest that metamorphic and igneous rocks tend to exhibit higher K_{sn} values, while sedimentary rocks generally have lower K_{sn} values (Fig. 7).

4.5. Correlation coefficients and PCA

Correlation analysis identified highly correlated ($r > 0.9$) morphometric and geomorphic parameters, with special emphasis on key variables such as area, perimeter, and river length. The matrix reveals that Lb is directly and positively correlated with basin A, P and Lu values, while being moderately and negatively correlated ($r > 0.85$) with Ff and Re (Fig. 8). Notable strong inverse relationships between Cc – Rc, Ccm – Dd, and Lg – Dd are also observed. Re, while correlating to a lesser extent ($r < 0.2$) with Hi, has a significant inverse ($r = -0.98$) correlation with Sh, which in turn has a significant positive correlation with Lb. Weak correlations exist between Dt and Rc, Rc and Dt; between Dt and Hi, Hi and Rbm; between Rbm and Fs. Likewise, a weak positive correlation ($r = 0.375$) was found between mean basin K_{sn} and rainfall across different stream orders (Fig. S4), while K_{sn} is moderately and positively correlated to HI and Rn.

PCA analysis of the enumerated 26 parameters revealed that six major principal components are responsible for 83.3% of the total variance (Table S2). PC1 accounts for 40.98% of the overall variance and is impacted by strongly loaded (>0.8) dimensional variables (A, P, Lb, Lu, Nu and Sh) (see Figure S5), followed by moderately loaded (>0.7) relief parameters (Dis, Bh, Rn). PC2, representing 20% of the total

variance, is influenced by significant loading (>0.8) of areal parameters (Dd, Fs and If), followed by HI (>0.5). PC3 demonstrates 6.9% of the total variance, through moderately loaded variables (Cc, Rbm and HI). PC4 explains 6.380%, influenced by Bs (>0.89) and Rr (>0.83). PC5 and PC6 account for 4.8% and 4% of the variance, respectively, with PC5 influenced by high K_{sn} (>0.8), rainfall (>0.6), and Dis (>0.4) values, while PC6 is mostly associated with Af (>0.8). Distinct clusters of the various sub-watersheds of different orders were discerned based on the PCA analysis and their graphical position denotes which morphometric attributes have fashioned their basin morphology.

4.6. Spatial distribution of knickpoints

Several rivers (Lawa, Sankh, South Koel, North Karo and South Karo) display major knickpoints associated with upstream lower-relief surface dissection in preserved Pleistocene 'very weak' to 'heavily weathered' lateritic caprock and early-Holocene alluvium (Fig. 9 and also Fig. S6 in the Supplementary Information). However, other rivers in the basin exhibit convex-up profiles characterized by minor knickpoints. A total of 154 knickpoints were identified through S-A and Chi (χ) profile analysis. A majority of them (72 or 47%), are located in Archean-Paleoproterozoic granite gneiss terrain (which is riven with joints and lineaments), followed by 17 (11%) in Archean Charnockites, and 16 (10%) in Archean-Paleoproterozoic quartzite (Fig. 10). Furthermore, observations reveal that most knickpoints have a height range or fall of 36 m to 97 m (i.e. difference between upper and lower elevation). The most prominent knickpoint is the Khandadhar waterfall (a horse-tail type fall, which is one of the highest in India), situated at a lithological boundary between 'moderately strong' banded hematite rocks (BIF) and 'very weak' phyllite. In all, 7 of the 14 highly prominent knickpoints (having fall >100 m above msl) are in areas underlain by granitic/gneissic rocks. Based on their relative position, 93 out of 154 knickpoints are classified as tectono-structurally originated, linked to faults (10), lineaments (9), thrusts (2), and joints/fractures (72). Furthermore, 53 knickpoints are formed due to variations in lithology and the remaining 8 are linked to dam construction in recent years (Fig. S7 and Fig. 6a). More specifically, 61 out of 154 knickpoints are

associated with waterfalls, originating from either lithological or tectono-structural influence, which can then be further classified as vertical step knickpoints (Fig. 6a).

4.7. Chi (χ) analysis

The Chi (χ) parameter is useful in determining the shift of a drainage divide, serving as an indication of prolonged bedrock erosion (Tucker and Whipple, 2002). Variations in Chi (χ) values correspond to the convexity and concavity developed along the river's longitudinal profile. The Chi (χ) values in the entire Brahmani Basin vary from 7.12 to 19098.22 (Fig. 11). Expectedly, most of the higher χ values were reported from higher elevation zones in the basin, further away from the its outlet (cf. Giachetta and Willett, 2018b; Joshi et al., 2021; Gemignani et al., 2022). Willett et al. (2014) state that river segments having higher χ values will have comparatively lower average channel steepness and lower erosivity (restated in Yang et al., 2022). matching with the pattern of basin-averaged K_{sn} values in our study, which are largely in the lower range in the upper catchment (Fig. 4h and Fig. 6). Furthermore, we have a quite interesting topographic configuration in the Brahmani Basin where radiometric dating ages in the upper catchment are almost four times younger than those in the middle part (Fig. S8). This middle section has incised channels through different metamorphics that comprise the Eastern Ghats (and also reports the largest grouping of higher basin-averaged K_{sn} values). In contrast, the upper catchment has large tracts of elevated pediplain-pediments formed over denuded Chotanagpur granite-gneiss (Fig. 2a, 2b). The relatively flatter terrain thus feasibly dampens channel slopes therein (i.e. lower K_{sn} and SL index values- Fig. 6). Higher χ values are detected in the upstream sections of Lawa, Sankh, South Koel, North Karo, and South Karo rivers, with lower χ values in the middle and downstream reaches of the Brahmani, Kurarhi, Tikera, and Nigra. A gradual decrease in χ values from north to south is apparent. Sub-watersheds (e.g. sw-1-20) located in the northeast part of the basin displays high χ values. The χ-elevation plots (χ-z) for the Brahmani and its selected major tributaries are given in Fig. 5 and Fig. S6.

The Lawa, with a m/n ratio of 0.53, is the river whose long profile is situated closest to the equilibrium steady state (Fig. S2). However, most of its tributaries exhibit notable convexity (zone of uplift or area gain) above 850 m asl, changing according to the landscape perturbations. Interestingly, similar m/n values were observed in the South Karo (m/n= 0.41) and Brahmani River (m/n= 0.40), but the upstream Brahmani (at >300 m asl) exhibits a more convex profile zone than South Karo's, and its middle reach (~250 m to ~100 m asl) shows a probable zone of erosion (Fig. 9). The profiles of most tributaries of the South Karo are parallel to the equilibrium line, signifying steady state, while most tributaries of the Brahmani (except some downstream reaches located at <100 m asl) are above the equilibrium line suggesting net gain in catchment area over incision at >300 m asl. Similarly, two downstream tributaries, Tikera (m/n= 0.33) and Nigra (m/n= 0.34) also represent convexity below the elevation of 100 m asl, while Tikera aggressively gains area at >200 m asl, with Nigra undergoing erosion. The χ-z plots of three rivers, Sankh (m/n= 0.36), North Karo (m/n= 0.35) and Kurarhi (m/n= 0.38) represent a step-like profile, indicating possible geological (lithological/structural) or anthropogenic disturbances. For example, the upper reach (at >400 m asl) of the Sankh has been gaining drainage area (aggressor), and its high χ values and low relief surface suggest possible river capture. In contrast, the upper reach of the North Karo (at >600 m asl) and Kurarhi (at >650 m asl) have experienced more erosion. The South Koel (m/n= 0.37) in its upstream reach (at >650 m asl) has experienced erosion, while its middle reach (650 m to ~450 m asl) exhibits a zone of convexity, along with lower relief landscape and moderate χ values, indicating minor river capture.

4.8. Reconstruction of probable paleo-drainage profiles

The reconstruction of the paleo-profile of a river can provide information about the total amount of incision that may have occurred and salient characteristics of the paleo-relief. The Sankh (S1) and South Koel (S2), were selected for this reconstruction analysis (Fig. 12). These two rivers meet at Vedavyas and flow as the Brahmani. These channels are controlled by two major knickpoints, with one common knickpoint in the lower reach near the break of slope. Both the upstream knickpoints are caused by modification of the base

level. The long profile of the Sankh (S1) has a mid-reach average concavity (θ) of 0.42 ± 0.086 and a normalized steepness index (K_{sn}) of 10.5 $m^{0.9}$, suggesting a net surface uplift/incision of 535 ± 33 m over time. At an elevation of 600 m, a knickpoint along the river divides it into two distinct segments, where the upper part exhibits a concave-up profile, which is typical of an eroded plateau. The middle reach of the South Koel (S2) has θ value of 0.38 ± 0.3 with corresponding K_{sn} of 4.94 $m^{0.9}$, suggesting a net surface uplift/incision of around 545 ± 30 m over time. The downstream common vertical step knickpoint of these two rivers, located along the main Brahmani channel, has θ of 0.59 ± 0.2 and higher K_{sn} value of 25.5 $m^{0.9}$, indicating possible transient adjustment with an incision depth of ~45 ± 8 m, and probable multiple phases of surface upliftment, similar to that reported from the nearby Eastern Bundelkhand craton (cf. Godin et al., 2023). However, dam construction near the natural slope break (completed in 1984), has complicated the river longitudinal profile character, making such landscape changes more difficult to discern discretely. The S-A analysis reconstructs paleo river profiles by tracing accumulation paths from the current river segments on each pixel, while χ analysis represents relict paleo-reaches by projecting slope intervals linearly. Our analysis indicates that the overall palaeo-relief in the Sankh River and South Koel River basins was likely to be ~508 m and ~520 m respectively, and the possible error range of just ~5% in these estimates showcases the reliability of this method.

5. Discussion

5.1. Geomorphometric characteristics of the sub-watersheds

Geomorphometric indices can help assess the influence of lithology, structure, climate, tectonics, eustasy and anthropogenic stresses on the landscape, indicating their pivotal role in terrain evolution over time (Ghasemlounia and Utlu, 2021; Taloor et al., 2021; Das et al. 2022; Solanki and Gupta, 2022; Diercks et al., 2023; Faisal and Hayakawa, 2023; Ghimire et al., 2023; Gururani et al., 2023). The study area is a good example of a half-graben, situated beside two major graben systems (the Koel-Damodar graben and the Mahanadi graben), truncated by the Kerajang Fault and NOBF. It is geologically complex due to

convergence of the Chotanagpur and Singhbhum microplates, that involves three tectonic cycles: (1) northward movement of the Singhbhum plate forming the Dalma Thrust Zone (2000–1600 Ma), (2) clockwise rotation causing a sinistral shear zone (1550–1170 Ma), and (3) NNW impingement creating the Singhbhum thrust zone (1000–850 Ma), with intervening periods of isostatic adjustments, upliftment, dyke intrusions, erosion, and sedimentation (Sarkar, 1982; Mahadevan, 2002; Chetty, 2014).

Rivers reshape landscapes through denudation, responding to these controlling factors, causing channel geometry modifications, erosive pulses and river captures, through a state of dynamic equilibrium. In all, 24 geomorphometric attributes of 280 sub-watersheds of the studied rivers helped to compare their hydro-geomorphic character. The relationships among such terrain variables, illustrated by their association with principal components, provides crucial insights into sub-watershed evolution (Sarkar and Patel, 2009, 2011, 2012). The PCA rotated matrix identified key parameters – Lb, Dd, Cc, Bs, K_{sn}, and Af – that significantly impact the landscape dynamics of the Brahmani Basin. It has also revealed strong correlations for A, P, Lb, Lu, Sh, Dd, Rr, K_{sn}, Bs, and Af across all components. Higher values of these strongly positively correlated variables are typically observed in higher order sub-watersheds, mostly characterized by moderately elevated pediment-pediplain surfaces and having dissected hills and valleys terrain. Further, the high Rn and Dis indices, complemented by high Bh and Nu values, suggest greater landscape erodibility in combination with greater runoff erosivity.

Further, PC2 highlighted the interrelationship between the strongly loaded hydrological variables (Dd, Fs and If) and the hypsometric integral (HI). Higher Dd values (>1.7 km/km^2) in the sub-watersheds sw-8, sw-47, and sw-49 are predominantly located around the elevated *Pat* regions of the Chotanagpur Plateau, displaying positive correlation with Fs and If, and negative correlation with CCM and Lg, suggesting potential landscape modification by denudation of lateritic terrain by surface runoff and leaching. Further, HI is positively correlated to channel steepness (K_{sn}) and basin relief, and inversely related to basin area, denoting the influence of fluvial incision in landscape change (Willgoose and Hancock, 1998; Donnaloia et al., 2019). Lower order sub-watersheds have more randomly scattered K_{sn}

versus precipitation plots and HI vs precipitation distribution, whereas slight positive relationship is observed in the higher order suggesting lesser impact of precipitation on the landscape (Fig. 8) (Guha and Jain, 2020; Banerjee et al., 2023). Most sub-watersheds are in mature stage (HI: 0 .1–0.4), highlighting the transitional stage of geomorphic evolution balanced stage between uplift and erosional process. Besides this, areas proximal to major faults in the Chotanagpur Gneissic Complex, Singhbhum orogenic belt, and Lower Gondwana zones, show higher HI (>0.5) and basin averaged K_{sn} values, with mean elevations nearing their maximum elevation, which is indicative of young transient sub-watersheds development due to major isostatic readjustments (upliftment, folds, faults, thrusts and shear zones) during the Neoproterozoic eon (~850 Ma) (cf. Sarkar, 1982).

PC3 is associated with moderately loaded variables (Cc and Rbm). The Brahmani River basin exhibits diverse drainage patterns, with radial patterns around the Chotanagpur gneissic complex hills, dendritic patterns in the lower deltaic-alluvial plains, and some trellis like patterns in the structurally complex Singhbhum craton region. Multiple sub-watersheds (sw-2, sw-19, sw-99, sw-109) in this region exhibit high R_{bm} values (>6) from 3rd and 4th order streams, indicating potential strong tectono-structural influence with high erosion susceptibility (cf. Nath et al., 2024). Typically, R_{bm} is positively correlated with the Re. However, here a negative correlation is observed, confirming the significant influence of past tectonics and more recent anthropogenic factors, in this highly dissected terrain (Bhat et al., 2020; Vanik et al., 2023). However, high Re in the Talcher basin indicates headward erosion probably because of the episodic reactivation of North Orissa Boundary Fault (NOBF) (Mukhopadhyay et al.,1984). PC4 is significantly influenced by higher loading of the basin slope (Bs) and relief ratio (Rr) parameters. Steep slopes may indicate fault scarps, whereas plains undergo sediment accumulation due to less slope gradient.

PC5 is influenced by high K_{sn} (r >0.8), Rainfall (r >0.6), and Dis (r >0.4) values, while PC6 is primarily associated with Af (r >0.8), denoting the probable role of inverse tectonics/seismicity induced basin tilting and litho-structural factors (Nexer et al. 2015). The mean basin K_{sn} and rainfall show a moderately positive correlation (r = 0.375), suggesting that lithological variations decently influence the

K_{sn}, while rainfall has lesser impact on it (Guha and Jain, 2020, Wang and Mudd, 2021, Moumeni et al., 2024). Higher K_{sn} and Af values correspond well with the distribution of recent seismic activity (Mw>4.0) and thermal springs, supporting the proposed hypothesis of inversion tectonism and deep-seated faults and shear zones (Fig. 3b). Besides this, the gravity anomalies associated with boundary faults suggest that such faults are deep-seated up to the basement in this region (cf. Subrahmanyam et al., 2008). It must also be noted that through the correlation and cluster analysis we have denoted how the various geomorphic parameters are related among themselves and combine in respect of different sub-watersheds. However, mere correlation does not necessarily imply direct causation and these relations may always translate into direct geomorphic action nor imply similar relationships with landscape dissection.

5.2. Climatic, litho-structural and anthropogenic drivers of river network morphology

Generally, lithological, tectono-structural, and anthropogenic factors collaboratively shape river morphologies and influence the evolution of river profiles, often leading to slope breaks in the longitudinal profiles of both trunk and tributary streams due to variations in structure and lithology (Crosby and Whipple, 2006; Willett et al., 2014; Stokes et al., 2017). Planar structures such as joints, fractures, veins, faults, and foliations formed due to tectonic stress and internal strain, play a significant role in the concurrent deformation of channels within this major granitic and minor basaltic complex (Dietrich et al., 1992; Ortega et al., 2014; Scott, 2015). The low relief relict landscape in the upper part of this basin helps in identifying such transient incisions through the derived parameters.

Swath profiles along trunk river channels demonstrate a general SE inclination of the basin, as per the regional slope. The basin experiences varying climates with annual precipitation ranging from 798 mm to 2365 mm, with the highest levels over the central highlands due to the orographic effect, followed by the coastal region. Variations in THi values have a negligible correlation with precipitation distribution, suggesting lesser impact of direct precipitation on river profiles. However, the longitudinal profiles indicate a slight positive correlation between K_{sn} values and precipitation, influencing channel incision (Guha and

Jain., 2020; Das et al., 2022). Asymmetric swath profiles denote depressions associated with multiple major and minor faults. Structures such as joints and fractures, caused by brittle deformation of the bedrock, exhibit lower resistance to erosion and thus, higher jointed bedrock density can enhance bedrock erosion rates (cf. Pelletier et al., 2009).

The K_{sn} values and knickpoints serve as effective geomorphological indicators for assessing bedrock erodibility and litho-structural impacts. A higher K_{sn} coupled with elevated local relief typically signals either local uplift or a historical fall in base level or reactivation of existing boundary faults (i.e., Bishop and Goldrick, 2010; Forte et al., 2014; Mohanty, 2023). A box and whisker plot shows the anomalies in K_{sn} associated with bedrock variations (Fig. 7), while Fig. 11 presents the distribution of knickpoints across various lithologies to assess the impacts of distinct rock types on these values. Similarly, pronounced and evident variations in the litho-structure framework influence SL and K_{sn} values, with higher values typically associated with sudden slope breaks near lithological boundaries (Fig. 6b and Figure S3). For instance, a significant increase in K_{sn} and SL values just below the downstream of Rengali Dam is likely due to the combined impact of the dam and the periodically reactivated Kerajang shear zone (550-500 Ma) and Barakot Fault (950-700 Ma) (Crowe et al., 2001; Gupta et al., 2021). Additionally, the presence of Permo-Triassic (~300 Ma) glaciogenic sediments alongside cyclothemic deposits in the Talcher basin signifies regional climatic transition from glacial to fluvial environment, further evidenced by variations in sediment grain size, mineral composition, and depositional structures (Crowe et al, 2001; Biswas, 2003).

Various researchers have found that numerous pre-existing faults, shear zones and thrusts in Indian Shield have been reactivated, such as the Great Boundary Fault, Son–Narmada Faults, Central Indian Shear, Gavilgarh-Tan Shear, Pokhara Fault, Tapti Fault Zone, Kodki fault zone (Chattopadhyay and Bhattacharjee, 2019; Godin et al, 2023; Kothyari et al., 2024). These reactivated shear zones along with some basement faults can feasibly cause localized tectonic perturbations and deformation, increasing river incision and steepness, thereby making it a seismic hazard prone region under Zone-III similar to locations like Latur (1993), Koyna (1967), Jabalpur (1997), Bhilai (1966), Kutch (2017) (dates of recent marked seismic events

in these locations are mentioned in the parentheses). As can be seen from Figure S8, there is a wide range in geological age across the basin. Interestingly, the northern portion near the *Pats* has younger dates (972 – 860 Ma), while the age increases steadily towards the central portion of the basin, where the river cuts southward across the hill ranges of the Eastern Ghats (oldest age of 3369 Ma), and exposes the older underlying strata (possibly creating a valley-inlier type of topography). Ages decline south of this, to 973 Ma where the river turns east towards the Bay of Bengal. The location of younger surfaces at higher elevation (viz. the northern *Pats*) denote the complex uplift history of the region. Furthermore, the oldest rocks in the central part of the basin still display marked relief and topography, despite the long-term denudation that they have undergone. This may be due to either continued/reactivated uplift in the region, as evidenced by the incised stream courses, high K_{sn} values and narrow floodplains.

Higher values (>25 $m^{0.9}$) of K_{sn} are reported from the granitic gneiss terrain of the Chotanagpur and Singhbhum belt, highly weathered dolerite outcrops, hard crystalline but fractured Charnockites of the Eastern Ghats group, epidiorite of Dalma metavolcanics; ultrabasic and ultramafic rock types. All these lithologies report relatively higher channel incision rates. Lower K_{sn} values (<10 $m^{0.9}$) are reported from the carbonaceous sandstone, compact clay, laterite, limestone, newer alluvium and pegmatite rock types (Fig. 6). Median K_{sn} values show identical differences across lithological types, possibly denoting that overall, the lithology alone has a limited influence on K_{sn} values and consequently, erosion rates. Fig. 13 (b, c) denotes the marked structural influence of dykes and other intrusives on drainage alignment (field photographs in Fig. S9) and K_{sn} values in the upper part of the Brahmani basin, where the two principal tributaries (South Koel and Sankh) meet to form the main river (Fig. 13a). Similar K_{sn} value ranges have been reported from other important peninsular rivers like the Subarnarekha and Aghnashini, along with several west flowing rivers of the Western ghats and Kachchh region (Guha and Patel, 2017; Guha and Jain, 2020; Das et al, 2022; Kothyari, 2022). Also, studies globally have consistently reported that the highest K_{sn} values are associated with hard metamorphic rocks such as gneiss and charnockite, while the lowest K_{sn} values are found in Cenozoic sedimentary rocks (Struth et al., 2019; Wang and Mudd, 2021).

In this study, 60% of all discerned knickpoints are structurally originated, highlighting the structural complexities of the region, while only 34% knickpoints that are linked to lithological factors act as a proxy for denoting the higher erodibility of the underlying bedrock (Fig. 9 and Fig. S6; Chilton and Spotila, 2022). Additionally, 40% the relatively higher altitude knickpoints (situated above100 m) in the upstream section correspond to vertical-step knickpoints (waterfalls), which are formed in response to local base level falls driven by tectono-structural controls (e.g. Kirby and Whipple, 2012; Campos et al., 2023). Channels characterized by waterfalls (Fig. S10), cascades and rapids often show high K_{sn} values along with greater lineament densities, and are also conduits for the substantial soil loss from the region during the monsoon. The Chotanagpur, Singhbhum and Eastern Ghats mobile belts, despite being parts of ancient cratons and terranes, are thus possibly episodically reactivated through tectonic/isostatic perturbations as evidenced by such structural knickpoints and seismic activities, with reference to recent lineament reactivation and incision rates (Gupta et al., 2014; Roychowdhury, 2019).

The highest number of knickpoints are found in highly crystalline granite gneiss, followed by Charnockite and quartzite rocks. The presence of sheet joints and fractures in the granitic gneiss complex accelerates the exfoliation process through physical and chemical weathering, resulting in porous and fragile rocks, ultimately being washed away by splash erosion and runoff (see field photographs in Fig. S11). Beside this, the presence of potholes in granitic bedrock (Fig. S12) corresponds well with some upstream knickpoints of the Sankh and South Koel rivers, confirming the influence of joints and fractures in facilitating erosion processes such as plucking, abrasion, weathering, and cavitation on highly resistant granitic rocks in long-term riverbed incision. Similarly, the recorded mean RockSchmidt hammer rebound values (Table S3) also confirm the generally low relative rock strength and weathered and weakly compacted nature of these lithological units. The highest number of knickpoints (44) are found at altitudes of 400-499 m, while only 14 knickpoints exist above 100 m (Tables S4-S5 in the Supplementary Information). The 300–600 m elevation zone constitutes the primary scarp faces of the region (separating the upper plateau surface from the pediplains/floodplains below), with notable breaks in slope, and thus

72% of all knickpoints are present in this range. It is possible that the lower-elevation knickpoints were potentially affected by Quaternary climate changes or recent base level changes (cf. Clementucci et al., 2023; Shen et al., 2023). Only 5% of knickpoints are associated with human impoundments (i.e. enforced local/temporary base level changes), with the most prominent vertical-step knickpoints coupling with spiked SL and K_{sn} values near major dams and barrages like the Rengali and Samal on the Brahmani River, Mandira on the Sankh, Laratu on the North Karo and Derjang on the Nigra River (it is also likely that the dams were set up in these locations taking advantage of harder underlying substrate, so dam-proximal SL and K_{sn} variations can also be taken to indicate litho-structural influences). Additionally, some knickpoints are found in to proximity to heavy iron mining activities in the South Karo and the Kurarhi river network, which may affect the local terrain and vegetation cover and thus influence discharge and channel morphology.

5.3. Rearrangement of drainage networks

The χ metric uses the linearity and slope of bedrock river profiles to predict a stable state, proportional to the channel's steepness (K_{sn}) (Whipple et al., 2007; Mudd et al., 2014). The χ plots highlighted that the Lawa River displays an almost linear trend and a convex form, showing minimal deviation from steady-state (E = U), suggesting that the river is nearly in the steady-state. The trunk channel of the Brahmani and the South Karo show a trend towards a linear yet concave form. Other bedrock rivers, i.e. Tikera, Nigra, Sankh, North Karo and Kurarhi are in more mature stages than the aforementioned streams, with concave form (Fig. 5 and Fig. S2). Furthermore, the low relief landscape in the upstream section of the Lawa, Sankh, South Koel, Norh Karo and South Karo rivers can be used to feasibly discern pre-uplift conditions and topographic rejuvenation, as evidenced by the presence of Pleistocene laterite caprock residuum and early-Holocene alluvium as paleo bedrock remnants (Fig. 5).

The χ-profile analysis also predicts the drainage system reorganization through fluvial incision by expanding the drainage area via headwater migration (Bhattarai et al., 2021). This occurs when a channel

segment with a lower χ value (i.e. a more erosive stream) captures a segment with a higher χ value (i.e. less erosive) at the drainage divide, indicating a shift in the drainage divide (denoted by arrows in Fig. 11) into the basin with higher χ values. Based on this, sub-watersheds are moving towards NW in the Lawa basin, north-eastwards in the Sankh, South Koel and North Karo basins, and towards SE in the South Karo basin. Several drainage divides of sub-watersheds (234, 236, 238, 250, and 275) near the Northern Boundary Fault (NOBF), Kerajang Shear Zone, Akul Fault and Malaygiri Lineament may have also been experiencing shifts due to subsurface reactivation (cf. Gupta et al., 2014; Pradhan and Jena, 2016).

This study reconstructs the paleo-profiles the two main tributaries of the Brahmani (Sankh and South Koel) channels, discerning almost similar initial surface uplift of ~510 m and ~520 m, respectively, and ~45 m in the main Brahmani channel section (Fig. 12). This upliftment is mainly along slope break knickpoints, indicating significant bedrock erosion. The South Koel River has had a relatively more intense geomorphological evolution due to higher incision rates, likely influenced by greater stream power, precipitation, and lithological variations. Lastly, the study also concludes that constructed dams can have a notable significance on the evolution of channels (albeit in a shorter timescale), alongside structural, lithological, and climatic factors (Slowik et al., 2018; Poeppl et al., 2019; You et al., 2022).

6. Conclusion

The Brahmani River basin has undergone several episodic tectonic/geological events through upliftment and reactivation of faults, during the Precambrian to Recent. Most of the relict landscapes of the Archaean have been altered by several deformations, erosional processes and Holocene anthropogenic activities. We have analysed the geomorphology of the Brahmani River Basin by computing geomorphometric indices, topographic swath profiles and fluvial metrics (SL, K_{sn}, Chi, and knickpoints) of river channels to systematically discern the sub-watershed character and reorganization of river networks. We surmise the following:

- Structural and lithological factors have marked control on the rearrangement of drainage networks in the Eastern Ghats region and across the Brahmani Basin. However, recent human activities can also cause notable changes.
- Several identified sub-watersheds have better correspondence with high values of fluvial metrics, indicating that geomorphometric parameters are closely linked to drainage rearrangements. Specifically, headwater displacement of knickpoints near lithological boundaries due to probable reactivation of faults, variations in lithological resistance, coupling with higher chi values, indicate a potential for significant river piracy events within the basin.
- Moreover, the Brahmani and its selected tributaries are currently in a steady-state equilibrium phase by balancing incision rates accordingly. However, the majority of downstream tributaries are progressing toward a late-mature stage.

These findings provide new insights into the geomorphic evolution of the Eastern Ghats Hill Range and its surroundings, along with the nature of river reaction to possible uplift instances. While our analysis is focused on the Brahmani basin, the methods used can be employed elsewhere and can be useful in reconstructing paleo-surfaces and past river profiles, aiding landscape evolution studies. Furthermore, these insights can also aid in assessing specific site susceptibility to the natural hazards occurring in the Brahmani Basin.

Acknowledgements

The authors are grateful to the various online data repositories (ESA portal for COP-DEM; GSI's Bhukosh portal and Google Earth) for providing the datasets used in this study. AR acknowledges the UGC for the JRF provided for doctoral work.

Data Availability

All data used in this study are feely available in the public domain.

References

Ahmed, M.F., David Rogers, J., Ismail, E.H. 2018. Knickpoints along the upper Indus River, Pakistan: an exploratory survey of geomorphic processes. Swiss Journal of Geosciences, 111, 191-204. https://doi.org/10.1007/s00015-017-0290-3

Banerjee, S., Das, S., Kandekar, A.M., Scaringi, G., Sangode, S.J., 2023. Scale-dependency, rainfall, and lithologic controls on the hypsometry of the Western Ghats, India. Journal of Earth System Science 132, 49. https://doi.org/10.1007/s12040-023-02068-3.

Bekker, A., Slack, J.F., Planavsky, N., Krapez, B., Hofmann, A., Konhauser, K.O., Rouxel, O.J. (2010) Iron formation: the sedimentary product of a complex interplay among mantle, tectonic, oceanic and biospheric processes. Economic Geology, 105, 467-508. https://doi.org/10.2113/gsecongeo.105.3.467

Bhat, M.A., Dar, T., Bali, B.S., 2020. Morphotectonic analysis of Aripal Basin in the North-Western Himalayas (India): An evaluation of tectonics derived from geomorphic indices. Quaternary International 568, 103–115. https://doi.org/10.1016/j.quaint.2020.10.032

Bhattarai, I., Gani, N.D., Xue, L. 2021. Geomorphological response of rivers to active tectonics along the Siwalik Hills, Midwestern Nepalese Himalaya. Journal of Mountain Science, 18(5), 1264-1294. https://doi.org/10.1007/s11629-020-6330-x

Bhattacharya, H.N., Chakraborty, I., Ghosh, K. (2007) Geochemistry of some banded iron-formations of the Archean supracrustals, Jharkhand-Orissa region, India. Journal of Earth System Science, 116(3), 245-259. https://www.ias.ac.in/article/fulltext/jess/116/03/0245-0259

Bian, S., Tan, X., Liu, Y., Fan, S., Gong, J., Zhou, C., Shi, F. and Murphy, M.A., 2024. Orographic rainfall drives the Himalaya drainage divide to move north. *Geomorphology*, *444*, 108952.

Bishop, P., Goldrick, G. 2010. Lithology and evolution of bedrock rivers in post-orogenic settings: constraints from the high-elevation passive continental margin of SE Australia. Geological Society London Special Publications, 346, 267-287. https://doi.org/10.1144/SP346.14

Biswas, S.K., 2003. Regional tectonic framework of the Pranhita–Godavari basin, India. Journal of Asian Earth Sciences, 21(6), 543-551. https://doi.org/10.1016/S1367-9120(02)00145-1.

Bookhagen, B. and Burbank, D.W., 2006. Topography, relief, and TRMM-derived rainfall variations along the Himalaya. *Geophysical Research Letters*, *33*(8), L08405. https://doi.org/10.1029/2006GL026037.

Boulton, S.J. Geomorphic response to differential uplift: river long profiles and knickpoints from Guadalcanal and Makira (Solomon Islands). Frontiers in Earth Science, 8, 10. https://doi.org/10.3389/feart.2020.00010

Boulton, S.J., Stokes, M., Mather, A.E. Transient fluvial incision as an indicator of active faulting and Plio-Quaternary uplift of the Moroccan High Atlas. Tectonophysics, 633, 16-33. https://doi.org/10.1016/j.tecto.2014.06.032

Brocard, G.Y., Van Der Beek, P.A., Bourlès, D.L., Siame, L.L. and Mugnier, J.L., 2003. Long-term fluvial incision rates and postglacial river relaxation time in the French Western Alps from ^{10}Be dating of alluvial terraces with assessment of inheritance, soil development and wind ablation effects. *Earth and Planetary Science Letters*, *209*(1-2), 197-214. https://doi.org/10.1016/S0012-821X(03)00031-1.

Brocard, G.Y., Willenbring, J.K., Miller, T.E., Scatena, F.N. 2016. Relict landscape resistance to dissection by upstream migrating knickpoints. Journal of Geophysical Research Earth Surface, 121(6), 1182-1203. https://doi.org/10.1002/2015JF003678

Bull, W.B. 2007. Tectonic Geomorphology of Mountains: A New Approach to Paleoseismology. Wiley.

Burbank and Pinter, 1999. Landscape evolution: the interactions of tectonics and surface processes. *Basin Research*, *11*(1), 1-6.

Burbank, D.W., Anderson, R.S. 2011. Tectonic Geomorphology. Wiley.

Campos, D.S. de, Santos, M. dos, Marques, K.P.P., Silva, A.C., Vidal-Torrado, P., 2023. Impact of tectonic topographic rejuvenation in landscapes with high bedrock/duricrust strength: Insights from geomorphic evidence in a post-rifted region (SE Brazil). Geomorphology 435, 108749. https://doi.org/10.1016/j.geomorph.2023.108749.

Chalov, S., Prokopeva, K., Magritsky, D., Grigoriev, V., Fingert, E., Habel, M., Juhls, B., Morgenstern, A., Overduin, P.P., Kasimov, N. 2023. Climate change impacts on streamflow, sediment load and carbon fluxes in the Lena River delta, Ecological Indicators, 157, 111252. https://doi.org/10.1016/j.ecolind.2023.111252

Chattopadhyay, A. and Bhattacharjee, D., 2019. Repeated reactivation of the Gavilgarh-Tan Shear Zone, Central India: implications for the tectonic survival of deep-seated intra-continental fault zones. *Journal of Asian Earth Sciences*, *186*, 104051. https://doi.org/10.1016/j.jseaes.2019.104051.

Chen, H.E., Chiu, Y.Y., Cheng, C.Y. and Chen, S.C., 2023. Knickpoints and Fixpoints: The evolution of fluvial morphology under the combined effect of fault uplift and dam obstruction on a soft bedrock river. *Earth Surface Dynamics Discussions*, *2023*, 1-29. https://doi.org/10.5194/esurf-2023-8.

Chen, Y.C., Sung, Q. and Cheng, K.Y., 2003. Along-strike variations of morphotectonic features in the Western Foothills of Taiwan: tectonic implications based on stream-gradient and hypsometric analysis. *Geomorphology*, *56*(1-2), 109-137. https://doi.org/10.1016/S0169-555X(03)00059-X.

Chetty, T.R.K. 2014. Deep crustal shear zones in the Eastern Ghats Mobile Belt, India: Gondwana correlations. Journal of Indian Geophysical Union, 18(1), 19-56. https://iguonline.in/journal/Archives/18-1/2chetty.pdf

Chilton, K.D., Spotila, J.A., 2022. Uncovering the Controls on Fluvial Bedrock Erodibility and Knickpoint Expression: A High-Resolution Comparison of Bedrock Properties Between Knickpoints and Non-Knickpoint Reaches. Journal of Geophysical Research: Earth Surface 127, e2021JF006511. https://doi.org/10.1029/2021JF006511.

Choudhuri, A., Mandal, S., Bumby, A., Pillai, S.S.K. 2023. Glacial sedimentation in Northern Gondwana: insights from the Talchir formation, Manendragarh, India. Geological Magazine, 160(6), 1228-1240. https://doi.org/10.1017/S0016756823000353

Clark, M.K., House, M.A., Royden, L.H., Whipple, K.X., Burchfiel, B.C., Zhang, X. and Tang, W., 2005. Late Cenozoic uplift of southeastern Tibet. *Geology*, *33*(6), pp.525-528.

Clementucci, R., Ballato, P., Siame, L.L., Faccenna, C., Racano, S., Torreti, G., Lanari, R., Leanni, L., Guillou, V., 2023. Transient response to changes in uplift rates in the northern Atlas-Meseta system (Morocco). Geomorphology 436, 108765. https://doi.org/10.1016/j.geomorph.2023.108765.

Clubb, F.J., Mudd, S.M., Schildgen, T.F., Van der Beek, P.A., Devrani, R., Sinclair, H.D. 2023. Himalayan valley-floor widths controlled by tectonically driven exhumation. Nature Geoscience, 16, 739-746. https://doi.org/10.1038/s41561-023-01238-8

Crosby, B.T., Whipple, K.X. 2006. Knickpoint initiation and distribution within fluvial networks:236 waterfalls in the Waipaoa River, North Island, New Zealand. Geomorphology, 82(1-2), 16-38. https://doi.org/10.1016/j.geomorph.2005.08.023

Crowe, W.A., Cosca, M.A., Harris, L.B., 2001. $^{40}Ar/^{39}Ar$ geochronolgy and Neoproterozoic tectonics along the northern margin of the Eastern Ghats Belt in north Orissa, India. Precambrian Research, 108(3-4), 237-266. https://doi.org/10.1016/S0301-9268(01)00132-2

Crowe, W.A., Nash, C.R., Harris, L.B., Leeming, P.M., Rankin, L.R. 2003. The geology of the Rengali Province: implications for the tectonic development of northern Orissa, India. Journal of Asian Earth Sciences, 21(7), 607-710. https://doi.org/10.1016/S1367-9120(02)00034-2

CWC (Central Water Commission) 2012. Integrated Hydrological Data Book (Non-classified River Basins). Central Water Commission, New Delhi.

CWC (Central Water Commission) and NRSC (National Remote Sensing Centre) 2014. Brahmani and Baitarini Basin. v2. Ministry of Water Resources, Govt. of India. Available at https://indiawris.gov.in/downloads/Brahmani%20and%20Baitarni%20Basin.pdf

Daly, M.C., Chorowicz, J. and Fairhead, J.D., 1989. Rift basin evolution in Africa: the influence of reactivated steep basement shear zones. *Geological Society, London, Special Publications*, *44*(1), pp.309-334.

Das, S., Kandekar, A.M., Sangode, S.J., 2022. Lithologic controls on geomorphic evolution of the Central Western Ghats: an example from the Aghnashini catchment, Karnataka, India. Journal of the Geological Society of India 98, 451–459. https://doi.org/10.1007/s12594-022-2001-6.

Das, S., Mukherjee, J., Bhattacharyya, S., Patel, P.P., Banerjee, A. (2022) Detection of groundwater potential zones using analytical hierarchical process (AHP) for a tropical river basin in the Western Ghats of India. Environmental Earth Sciences, 81, 416. https://doi.org/10.1007/s12665-022-10543-1

Das, S., Sangode, S.J., Kandekar, A.M. 2021. Recent decline in streamflow and sediment discharge in the Godavari Basin, India (1965-2015). Catena, 206, 105537. https://doi.org/10.1016/j.catena.2021.105537

Das, S., Patel, P.P., Sengupta, S. (2016) Evaluation of different Digital Elevation Models for analyzing drainage morphometric parameters in a mountainous terrain: A case study of the Supin - Upper Tons Basin, Indian Himalayas", *SpringerPlus*, 5 (1544). https://doi.org/10.1186/s40064-016-3207-0

Delcaillau, B., Graveleau, F., Saint Carlier, D., Rao, G., Le Béon, M., Charreau, J. and Nexer, M., 2022. Geomorphic analysis of active fold growth and landscape evolution in the central Qiulitage fold belt, southern Tian Shan, China. *Geomorphology*, *398*, 108063.

Diercks, M.L., Grützner, C., Welte, J. and Ustaszewski, K., 2023. Challenges of geomorphologic analysis of active tectonics in a slowly deforming karst landscape (W Slovenia and NE Italy). *Geomorphology*, *440*, 108894.

Divyadarshini, A. and Singh, V., 2017. Identifying active structures in the Chitwan Dun, Central Nepal, using longitudinal river profiles and SL index analysis. *Quaternary International*, *462*, 176-193.

Donnaloia, M., Giachetta, E., Capolongo, D., Pennetta, L., 2019. Evolution of fluviokarst canyons in response to the Quaternary tectonic uplift of the Apulia Carbonate Platform (southern Italy): Insights from morphometric analysis of drainage basins. Geomorphology 336, 18–30. https://doi.org/10.1016/j.geomorph.2019.03.008.

Duvall, A., Kirby, E., Burbank, D. 2004. Tectonic and lithologic controls on bedrock channel profiles and processes in coastal California. Journal of Geophysical Research, 109, F03002. doi:10.1029/2003JF000086

East, A.E., Sankey, J.B. 2020. Geomorphic and sedimentary effects of modern climate change: current and anticipated future conditions in the western United States. Reviews of Geophysics, 58(4), e2019RG000692. https://doi.org/10.1029/2019RG000692

Fan, N., Chu, Z., Jiang, L., Hassan, M.A., Lamb, M.P., Liu, X. 2018. Abrupt drainage basin reorganisation following a Pleistocene river capture. Nature Communications, 9, 3756. https://doi.org/10.1038/s41467-018-06238-6

Ferreira de Lima, V., Furrier, M., Marques da Silva, R., Santos, C.A.G. 2024. Morphostructural influence and neotectonic activity in the geomorphological configuration of southeast Paraiba and northeast Pernambuco, Brazil. Heliyon, 10(9), e30111. https://doi.org/10.1016/j.heliyon.2024.e30111

Flint, J.J., 1974. Stream gradient as a function of order, magnitude, and discharge. *Water Resources Research*, *10*(5), 969-973.

Forte, A.M., Cowgill, E. and Whipple, K.X., 2014. Transition from a singly vergent to doubly vergent wedge in a young orogen: The Greater Caucasus. *Tectonics*, *33*(11), 2077-2101. https://doi.org/10.1002/2014TC003651.

Franks, S., Rengarajan, R. 2023. Evaluation of Copernicus-DEM and comparison to the DEM used for Landsat Collection-2 processing. Remote Sensing, 15(10), 2509. https://doi.org/10.3390/rs15102509

Gailleton, B., Mudd, S.M., Clubb, F.J., Grieve, S.W. and Hurst, M.D., 2021. Impact of changing concavity indices on channel steepness and divide migration metrics. *Journal of Geophysical Research: Earth Surface*, *126*(10), e2020JF006060. https://doi.org/10.1029/2020JF006060

Gailleton, B., Mudd, S.M., Clubb, F.J., Peifer, D., Hurst, M.D. 2019. A segmentation approach for the reproducible extraction and quantification of knickpoints from river long profiles. Earth Surface Dynamics, 7(1), 211-230. https://doi.org/10.5194/esurf-7-211-2019

Gailleton, B., Sinclair, H.D., Mudd, S.M., Graf, E.L.S. and Mațenco, L.C., 2021. Isolating lithologic versus tectonic signals of river profiles to test orogenic models for the Eastern and Southeastern Carpathians. *Journal of Geophysical Research: Earth Surface*, *126*(8), e2020JF005970. https://doi.org/10.1029/2020JF005970.

Gallen, S.F., Wegmann, K.W. and Bohnenstiehl, D.R., 2013. Miocene rejuvenation of topographic relief in the southern Appalachians. *GSA Today*, *23*(2), 4-10.

Gemignani, L., Mittelbach, B.V., Simon, D., Rohrmann, A., Grund, M.U., Bernhardt, A., Hippe, K., Giese, J., Handy, M.R. 2022. Response of drainage pattern and basin evolution to tectonic and climatic changes along the Dinarides-Hellenides orogen. Frontiers in Earth Science, 10, 821707. https://doi.org/10.3389/feart.2022.821707

Ghasemlounia, R., Utlu, M., 2021. Flood prioritization of basins based on geomorphometric properties using principal component analysis, morphometric analysis and Redvan's priority methods: A case study of Harşit River basin. Journal of Hydrology, 603, 127061. https://doi.org/10.1016/j.jhydrol.2021.127061.

Ghimire, M., Watanabe, T., Evans, I.S., 2024. Geomorphological significance of the morphometric characteristics of first-order basins in the Siwalik Hills in the Himalayas, Nepal. Physical Geography 45, 231–266. https://doi.org/10.1080/02723646.2023.2216954.

Giachetta E., Willett, S.D. 2018b, A global dataset of river network geometry. Scientific Data, 5, 180127. https://doi.org/10.1038/sdata.2018.127

Giachetta E., Willett, S.D. 2018a. Effects of River Capture and Sediment Flux on the Evolution of Plateaus: Insights From Numerical Modeling and River Profile Analysis in the Upper Blue Nile Catchment. Journal of Geophysical Research: Earth Surface, 123(6), 1187-1217. https://doi.org/10.1029/2017JF004252

Gilbert, G.K., 1877. *Geology of the Henry Mountains* (pp. i-160). Government Printing Office, US.

Godin, L., Crilly, B., Schoenbohm, L.M. and Wolpert, J., 2023. Recent basement fault reactivation and fluvial drainage modification in an intraplate setting, eastern Bundelkhand Craton, Madhya Pradesh, India. *Geomorphology*, *436*, 108781. https://doi.org/10.1016/j.geomorph.2023.108781.

González Moradas, M.D.R., Viveen, W., Vidal Villalobos, R.A. and Villegas Lanza, J.C., 2023. A performance comparison of SRTM v. 3.0, AW3D30, Aster GDEM3, Copernicus and Tandem-x for tectonogeomorphic analysis in the south American Andes. *Catena*, 228, 107160.

Goudie, A.S. 2006. The Schmidt Hammer in geomorphological research. Progress in Physical Geography: Earth and Environment, 30(6), 703-718. https://doi.org/10.1177/0309133306071954

Grabowski, R.C., Vercruysse, K., Holman, I., Azhoni, A., Bala, B., Shankar, V., Beale, J., Mukate, S., Poddar, A., Peng, J., Meersmans, J. 2022. The land-river interface: a conceptual framework of environmental process interactions to support sustainable development. Sustainability Science, 17, 1677-1693. https://doi.org/10.1007/s11625-022-01150-x

GSI (Geological Survey of India) 2012. Briefing Book of Eastern Region. GSI, Kolkata.

Guha, S. and Jain, V., 2020. Role of inherent geological and climatic characteristics on landscape variability in the tectonically passive Western Ghat, India. *Geomorphology*, *350*, 106840. https://doi.org/10.1016/j.geomorph.2019.106840.

Guha, S. and Patel, P.P., 2017. Evidence of topographic disequilibrium in the Subarnarekha River Basin, India: A digital elevation model-based analysis. *Journal of Earth System Science*, *126*, 1-20.

Gupta, S., Mohanty, W.K., Mandal, A., Misra, S. 2014. Ancient terrane boundaries as probable seismic hazards: a case study from the northern boundary of the Eastern Ghats Belt, India. Geoscience Frontiers, 5(1), 17-24. https://doi.org/10.1016/j.gsf.2013.04.001

Gururani, K., Kothyari, G.C., Kotlia, B.S., 2023. Morphotectonic assessment of the Gaula river basin, Kumaun lesser Himalaya, Uttarakhand. Quaternary Science Advances 12, 100115. https://doi.org/10.1016/j.qsa.2023.100115.

Guth, P.L., Geoffroy, T.M. 2021 LiDAR point cloud and ICESat-2 evaluation of 1 second global digital elevation models: Copernicus wins. Transactions in GIS, 25(5), 2245-2261. https://doi.org/10.1111/tgis.12825

Guth, P.L., Trevisani, S., Grohman, C.L., Lindsay, J., Gesch, D., Hawker, Bielski, C. 2024. Ranking of 10 Global One-Arc-Second reveals limitations in terrain morphology representation. Remote Sensing, 16(17), 3273. https://doi.org/10.3390/rs16173273

Hack, J.T., 1973. Stream-profile analysis and stream-gradient index. *Journal of Research of the US Geological Survey*, *1*(4), 421-429.

Harel, M.-A., Mudd, S.M., Attal, M. 2016. Global analysis of the stream power law parameters based on worldwide ^{10}Be denudation rates. Geomorphology, 268, 184-196. https://doi.org/10.1016/j.geomorph.2016.05.035

Haviv, I., Enzel, Y., Whipple, K.X., Zilberman, E., Matmon, A., Stone, J. and Fifield, K.L., 2010. Evolution of vertical knickpoints (waterfalls) with resistant caprock: Insights from numerical modeling. *Journal of Geophysical Research: Earth Surface*, *115*(F3), F03028. https://doi.org/10.1029/2008JF001187.

He, C., Braun, J., Tang, H., Yuan, X., Acevedo-Trejos, E., Ott, R.F., De Quay, G.S. 2024. Drainage divide migration and implications for climate and biodiversity. Nature Reviews Earth and Environment, 5, 1177-192. https://doi.org/10.1038/s43017-023-00511-z

Hergarten, S. 2021. The influence of sediment transport on stationary and mobile knickpoints in river profiles. Journal of Geophysical Research Earth Surface, 126(12), e2021JF006218. https://doi.org/10.1029/2021JF006218

Jaiswal, K. and Sinha, R., 2007. Probabilistic seismic-hazard estimation for peninsular India. *Bulletin of the Seismological Society of America*, *97*(1B), 318-330.

Jaiswara, N.K., Kotluri, S.K., Pandey, P., Pandey, A.K., 2020. MATLAB functions for extracting hypsometry, stream-length gradient index, steepness index, chi gradient of channel and swath profiles

from digital elevation model (DEM) and other spatial data for landscape characterisation. Applied Computing and Geosciences 7, 100033. https://doi.org/10.1016/j.acags.2020.100033.

Jaiswara, N.K., Pandey, P., Pandey, A.K. 2019. Mio-Pliocene piracy, relict landscape and drainage reorganization in the Namcha Barwa syntaxis zone of eastern Himalaya. Scientific Reports, 9(1), 17585. https://doi.org/10.1038/s41598-019-54052-x

Jancewicz, K., Rozycka, M., Szymanowski, M., Kryza, M., Migon, P. 2022. Topographic Characteristics of Drainage Divides at the Mountain-Range Scale—A Review of DTM-Based Analytical Tools. ISPRS International Journal of Geo-Information, 11(2), 116. https://doi.org/10.3390/ijgi11020116

Jansen, J.D., Codilean, A.T., Bishop, P., Hoey, T.B. 2010. Scale dependence of lithological control on topography: bedrock channel geometry and catchment morphometry in Western Scotland. The Journal of Geology, 118(3), 223-246. https://doi.org/10.1086/651273

Jena, R., Pradhan, B., Alamri, A.M., Susceptibility to seismic amplification and earthquake probability estimation using recurrent neural network (RNN) model in Odisha, India. Applied Sciences, 10(15), 5355. https://doi.org/10.3390/app10155355

Joshi, N., Kothyari, G.C. and Pant, C.C., 2021. Drainage conformation and transient response of river system in thrust segmentation of Northwest Himachal Himalaya, India. *Quaternary International*, *575*, 37-50. https://doi.org/10.1016/j.quaint.2020.05.024

Kale, V.S. 1999. Long-period fluctuations in monsoon floods in the Deccan Peninsula, India. Journal of the Geological Society of India, 53, 5-15.

Kale, V.S. 2002. Fluvial geomorphology of Indian Rivers: an overview. Progress in Physical Geography, 26(3), 400-433. https://doi.org/10.1191/0309133302pp343ra

Kale, V.S. 2003. Geomorphic effects of monsoon floods on Indian Rivers. Natural Hazards, 28, 65-84. https://doi.org/10.1023/A:1021121815395

Kale, V.S. and Shejwalkar, N., 2008. Uplift along the western margin of the Deccan Basalt Province: Is there any geomorphometric evidence?. *Journal of Earth System Science*, *117*, 959-971.

Kashyap, A., Pandey, A.K., Behera, M.D. 2024. Mio-Pliocene paleo-course of Indus River in Upper Sutlej-Zhada basin: Implication of tectonic uplift on river piracy and drainage reorganization in SW Tibet and NW Himalaya. Earth Surface Processes and Landforms, 49(13), 4428-4443. https://doi.org/10.1002/esp.5977

Kaveh-Firouz, A., Burg, J-P., Giachetta, E. 2024. Landscape evolution in orogenic plateaus: Insights from quantitative morphotectonic analysis of the Turkish–Iranian Plateau and Caucasus regions. Earth Surface Processes and Landforms, 49(3), 1214-1238. https://doi.org/10.1002/esp.5756

Keller, E.A., Pinter, N. 2002. Active Tectonics: earthquakes, uplift, and landscape. Prentice-Hall, New Jersey.

Khan, S., Sinha, R., Whitehead, P., Sarkar, S., Jin, L., Futter, M.N. 2018. Flows and sediment dynamics in the Ganga River under present and future climate scenarios. Hydrological Sciences Journal, 63(5), 763-782. https://doi.org/10.1080/02626667.2018.1447113

Kirby, E. and Whipple, K.X., 2001. Quantifying differential rock-uplift rates via stream profile analysis. Geology, 29(5), 415-418. https://doi.org/10.1130/0091-7613(2001)029%3C0415:QDRURV%3E2.0.CO;2

Kirby, E. and Whipple, K.X., 2012. Expression of active tectonics in erosional landscapes. *Journal of Structural Geology*, *44*, 54-75. https://doi.org/10.1016/j.jsg.2012.07.009

Köppen, W.P., 1931. *Grundriss der klimakunde*. W. de Gruyter.

Korup, O., Densmore, A.L. and Schlunegger, F., 2010. The role of landslides in mountain range evolution. *Geomorphology*, *120*(1-2), pp.77-90.

Kothyari, G.C., Jani, C., Bajpai, S., Lakhote, A., Chauhan, G., Agrawal, K., Dumka, R., Shukla, A., Kandregula, R.S., Sairam, B. and Thakkar, M., 2024. Bed parallel slip and paleostress analysis of the Kodki fault zone, Kachchh, Western India. *Quaternary Science Advances*, *13*, 100137. https://doi.org/10.1016/j.qsa.2023.100137.

Kothyari, G.C., Kotlia, B.S., Talukdar, R., Pant, C.C. and Joshi, M., 2020. Evidences of neotectonic activity along Goriganga river, higher central Kumaun Himalaya, India. *Geological Journal*, *55*(9), pp.6123-6146. https://doi.org/10.1002/gj.3791.

Kothyari, G.C., Mishra, S., Taloor, A.K., Kandregula, R.S., Pathak, V. and Chauhan, G., 2022. Distribution of neotectonic variability between the Kachchh mainland fault and Vigodi fault, northwestern mainland Kachchh, western India. *Quaternary Science Advances* 6, 100047, https://doi.org/10.1016/j.qsa.2021.100047

Lague, D. 2014. The stream power river incision model: evidence, theory and beyond. Earth Surface Processes and Landforms, 39, 38-61. https://doi.org/10.1002/esp.3462

Leister-Taylor, V., Jacob P., Schrader H., and Kahabka H., 2020. Copernicus DEM Validation Report. November 9. https://spacedata.copernicus.eu/documents/20126/0/GEO1988-CopernicusDEM-RP-001_ValidationReport_I3.0.pdf.

Leonard, J.S. and Whipple, K.X., 2021. Influence of spatial rainfall gradients on river longitudinal profiles and the topographic expression of spatially and temporally variable climates in mountain landscapes. *Journal of Geophysical Research: Earth Surface*, *126*(12), e2021JF006183. https://doi.org/10.1029/2021JF006183.

Li, J., Wang, G., Song, C., Sun, S., Ma, J., Wang, Y., Guo, L., Li, D. 2024. Recent intensified erosion and massive sediment deposition in Tibetan Plateau rivers. Nature Communications, 15, 722. https://doi.org/10.1038/s41467-024-44982-0

Li, Z., Chen, J., Han, M., Li, Y., Cao, C., Song, S., Zhang, Y., Yan, J. 2021. Distribution and evolution of knickpoints along the Layue River, Eastern Himalayan Syntaxis. Journal of Hydrology, 603(A), 126915. https://doi.org/10.1016/j.jhydrol.2021.126915

Lima, A.G., Binda, A.L. 2013. Lithologic and structural controls on fluvial knickzones in basalts of the Parana Basin, Brazil. Journal of South American Earth Sciences, 48, 262-270. https://doi.org/10.1016/j.jsames.2013.10.004

Luo, Q., Schoenbohm, L., Rimando, J., Li, Y., Li, C. and Xiong, J., 2023. Morphometric analysis of the North Liuleng Shan Fault in the northern Shanxi Graben System, China: Insights into active deformation pattern and fault evolution. *Geomorphology*, *440*, 108862.

Luppichini, M., Lazzarotti, M., Bini, M., Climate change as main driver of centennial decline in river sediment transport across the Mediterranean region. Journal of Hydrology, 636, 131266. https://doi.org/10.1016/j.jhydrol.2024.131266

Mackin, J. H. 1948. Concept of the graded river, Bulletin of the Geological Society of America, 59, 463-512.

Mahadevan, T.M. 2002. Geology of Bihar and Jharkhand. Geological Society of India, Bengaluru.

Majhi, A., Shaw, R., Mullick, K., Patel, P.P. (2021) Towards improved USLE-based soil erosion modelling in India: A review of prevalent pitfalls and implementation of exemplar methods. *Earth-Science Reviews* 221, 103786. https://doi.org/10.1016/j.earscirev.2021.103786

Mishra, S.K. 2002. Development Displacement: A case study of Rengali Dam in Orissa, India. PhD Thesis, University of Hyderabad, India. Available at https://dspace.uohyd.ac.in/server/api/core/bitstreams/75c22e31-1a28-4998-abe8-37339007eb8f/content

Mitchell, N.A., Yanites, B.J. 2021. Bedrock river erosion through dipping layered rocks: quantifying erodibility through kinematic wave speed. Earth Surface Dynamics, 9, 723-753. https://esurf.copernicus.org/articles/9/723/2021/

Mohanty, S.P. 2023. Structural and tectonic analyses of the Chhotanagpur Gneiss Complex of the Eastern Satpura Orogen, India: Significance for a global model. Geosystems and Geoenvironment, 2(4), 100202. https://doi.org/10.1016/j.geogeo.2023.100202

Mol, L. 2014. Measuring rock hardness in the field. In: British Society for Geomorphology (BSG) (eds.) Geomorphological Techniques, sec. 3.2. https://www.geomorphology.org.uk/app/uploads/2024/02/BSG-Geomorphology-Techniques.pdf

Molin, P., Pazzaglia, F.J. and Dramis, F., 2004. Geomorphic expression of active tectonics in a rapidly-deforming forearc, Sila massif, Calabria, southern Italy. *American Journal of Science*, *304*(7), 559-589.

Moumeni, M., Delchiaro, M., Della Seta, M., Nozaem, R., Ballato, P., Leonard, J.S., Clementucci, R. and Rouhi, J., 2024. Interplay between tectonics and surface processes in the evolution of mountain ranges: Insights from landscape dynamics, uplift, and active deformation of Talesh Mountains (NW Iranian Plateau margin). *Geomorphology*, *448*, 109029. https://doi.org/10.1016/j.geomorph.2023.109029

Mudd, S.M., Attal, M., Milodowski, D.T., Grieve, S.W. and Valters, D.A., 2014. A statistical framework to quantify spatial variation in channel gradients using the integral method of channel profile analysis. *Journal of Geophysical Research: Earth Surface*, *119*(2), 138-152. https://doi.org/10.1002/2013JF002981.

Mudd, S.M., Clubb, F.J., Gailleton, B., Hurst, M.D. 2018. How concave are river channels? Earth Surface Dynamics, 6(2), 505-523. https://esurf.copernicus.org/articles/6/505/2018/

Mukherjee, J., Patel, P.P. (2022) Landscape Characterization using Geomorphometric Parameters for a Small Sub-Humid River Basin of the Chota Nagpur Plateau, Eastern India. In: Shit P.K., Bera B., Islam A., Ghosh S., Bhunia G.S. (eds) Drainage Basin Dynamics: An Introduction to Morphology, Landscape and Modelling. Springer, Cham, pp. 127-152. https://link.springer.com/chapter/10.1007/978-3-030-79634-1_6

Mukherjee, S., Dey, A., Sanyal., S., Sengupta, P. 2019. Proterozoic Crustal Evolution of the Chotanagpur Granite Gneissic Complex, Jharkhand-Bihar-West Bengal, India: Current Status and Future Prospect. In: Mukherjee, S. (ed.) Tectonics and Structural Geology: Indian Context. Springer, Cham, pp. 7-54. https://doi.org/10.1007/978-3-319-99341-6_2

Mukhopadhyay, D., 1984. The Singhbhum shear zone and its place in the evolution of the Precambrian mobile belt of North Singhbhum. Indian J. Earth Sci., 205–212.

Mukhopadhyay, G., Mukhopadhyay, S.K., Roychowdhury, M., Parui, R.K. 2010. Stratigraphic correlation between different Gondwana Basins of India. Journal of the Geological Society of India, 76, 251-266. https://doi.org/10.1007/s12594-010-0097-6

Nath, K., Halder, S., Gogoi, D., Mahanta, B.N., Goswami, T.K., Sarma, R.K., 2024. Neotectonism and reactivation of tectonic elements in eastern part of Shillong Plateau, India: constraints from morpho-tectonic analyses. Geology, Ecology, and Landscapes. https://doi.org/10.1080/24749508.2024.2338973.

Naylor, L.A., Spencer, T., Lane, S.N., Darby, S.E., Magilligan, F.J., Macklin, M.G., Moller, I. 2017. Stormy geomorphology: geomorphic contributions in an age of climatic extremes. Earth Surface Processes and Landforms, 42(1), 166-190. https://doi.org/10.1002/esp.4062

Neely, A.B., Bookhagen, B. and Burbank, D.W., 2017. An automated knickzone selection algorithm (KZ-Picker) to analyze transient landscapes: Calibration and validation. *Journal of Geophysical Research: Earth Surface*, *122*(6), 1236-1261. https://doi.org/10.1002/2017JF004250.

Negi, P., Goswami, A. and Joshi, G.C., 2023. Geomorphic indices based topographic characterization of Alaknanda catchment, Western Himalaya using spatial data. *Environmental Earth Sciences*, *82*(20), 468.

Nexer, M., Authemayou, C., Schildgen, T., Hantoro, W.S., Molliex, S., Delcaillau, B., Pedoja, K., Husson, L. and Regard, V., 2015. Evaluation of morphometric proxies for uplift on sequences of coral reef terraces: a case study from Sumba Island (Indonesia). *Geomorphology*, *241*, 145-159. https://doi.org/10.1016/j.geomorph.2015.03.036.

Ortega, J.A., Gómez-Heras, M., Perez-López, R. and Wohl, E., 2014. Multiscale structural and lithologic controls in the development of stream potholes on granite bedrock rivers. *Geomorphology*, *204*, 588-598. https://doi.org/10.1016/j.geomorph.2013.09.005.

Panda, D.K., Kumar, A. and Mohanty, S., 2011. Recent trends in sediment load of the tropical (Peninsular) river basins of India. *Global and Planetary Change*, *75*(3-4), pp.108-118.

Patel, P.P. (2013): GIS Techniques for Landscape Analysis - Case Study of the Chel River Basin, West Bengal. *Proceedings of State Level Seminar on Geographical Methods in the Appraisal of Landscape,*

held at Dept. of Geography, Dum Dum Motijheel Mahavidyalaya, Kolkata, on 20th March, 2012, pp. 1-14.

Patel, P.P., Dasgupta, R., Chanda, S., Mondal, S. (2021a) An investigation into longitudinal forms of gullies within the "Grand Canyon" of Bengal, Eastern India. *Transactions in GIS* 25(5), 2501-2528. https://doi.org/10.1111/tgis.12828

Patel, P.P., Guha, S., Das, D. and Bose, M., 2022. Spatial variability of topographic attributes and channel morphological characteristics in the Ladakh Trans-Himalayas and their tectonic and structural controls. In *Himalayan Neotectonics and Channel Evolution* (pp. 67-110). Cham: Springer International Publishing. https://doi.org/10.1007/978-3-030-95435-2_3

Patel, P.P., Mondal, S., Dasgupta, R. (2021b). Morphometric and channel erosivity analysis of lateritic gully catchments using high resolution DTM and repeat survey structure-from-motion datasets. In M. Alvioli, I. Marchesini, L. Melelli P. Guth (Eds.), GEOMORPHOMETRY 2020 Conference Proceedings (pp. 251-253). Perugia: CNR Edizioni. https://www.irpi.cnr.it/conference-files/geomorphometry-2020/67.pdf

Patel, P.P., Sarkar, A. (2010): Terrain Characterization Using SRTM Data. *Journal of the Indian Society of Remote Sensing* 38(1), 11-24. https://doi.org/10.1007/s12524-010-0008-8

Pathak, V., Pant, C.C., Darmwal, G.S. 2015. Geomorphological features of active tectonics and ongoing seismicity of northeastern Kumaun Himalaya, Uttarakhand, India. Journal of Earth System Science, 124, 1143-1157. https://doi.org/10.1007/s12040-015-0611-8

Pelletier, J.D., Engelder, T., Comeau, D., Hudson, A., Leclerc, M., Youberg, A. and Diniega, S., 2009. Tectonic and structural control of fluvial channel morphology in metamorphic core complexes: The example of the Catalina-Rincon core complex, Arizona. *Geosphere*, *5*(4), pp.363-384.

Pérez-Peña, J.V., Al-Awabdeh, Mohammad, Azañón, J.M., Galve, J.P., Booth-Rea, G. and Notti, D., 2017. SwathProfiler and NProfiler: Two new ArcGIS Add-ins for the automatic extraction of swath and

normalized river profiles. *Computers and Geosciences*, *104*, 135-150. https://doi.org/10.1016/j.cageo.2016.08.008.

Perron, J.T. and Royden, L., 2013. An integral approach to bedrock river profile analysis. *Earth surface processes and landforms*, *38*(6), 570-576. https://doi.org/10.1002/esp.3302.

Peyerl, W.R., Salamuni, E., Queiroz, G.L., Silva, C.L. and Garcia, V.H., 2023. Identification of morphostructures by utilizing Knickpoint Ranks, a method to avoid the camouflage effect in knickpoint analysis. *Geomorphology*, *442*, 108919.

Phillips, J.D., McCormack, S., Duan, J., Russo, J.P., Schumacher, A.M., Tripathi, G.N., Brockman, R.B., Mays, A.B., Pulugurtha, S. Origin and interpretation of knickpoints in the Big South Fork River Basin, Kentucky-Tennessee. Geomorphology, 114(3), 188-198. https://doi.org/10.1016/j.geomorph.2009.06.023

Piacentini, D., Troiani, F., Servizi, T., Nesci, O., Veneri, F. 2020. SLiX: A GIS Toolbox to Support Along-Stream Knickzones Detection through the Computation and Mapping of the Stream Length-Gradient (SL) Index. ISPRS International Journal of Geoinformation, 9(2), 69. https://doi.org/10.3390/ijgi9020069

Poeppl., R.E., Coulthard, T., Keesstra, S.D., Keiler, M. 2019. Modeling the impact of dam removal on channel evolution and sediment delivery in a multiple dam setting, International Journal of Sediment Research, 34(6), 537-549. https://doi.org/10.1016/j.ijsrc.2019.06.001

Pradhan, B., Jena, R. 2016. Spatial relationship between earthquakes, hot-springs and faults in Odisha, India. IOP Conf. Series: Earth and Environmental Science, 37, 012070. doi:10.1088/1755-1315/37/1/012070

Pradhan, C., Chembolu, V., Dutta, S. 2019. Impact of river interventions on alluvial channel morphology. *ISH Journal of Hydraulic Engineering*, 25, 87-93. https://doi.org/10.1080/09715010.2018.1453878

Pradhan, C., Chembolu, V., Dutta, S., Bharti, R. 2021. Role of effective discharge on morphological changes for a regulated microchannel system. *Geomorphology*, 385, 107718. https://doi.org/10.1016/j.geomorph.2021.107718

Rai, D., Pattnaik, S., Rajesh, P.V. and Hazra, V., 2019. Impact of high resolution sea surface temperature on tropical cyclone characteristics over the Bay of Bengal using model simulations. *Meteorological Applications*, *26*(1), 130-139.

Rajasekhar, R.P., Mishra, D.C. 2008. Crustal structure of Bengal Basin and Shillong Plateau: Extension of Eastern Ghat and Satpura Mobile Belts to Himalayan fronts and seismotectonics. Gondwana Research, 14(3), 523-534. https://doi.org/10.1016/j.gr.2007.10.009

Rohrmann, A., Kirby, E., Schwanghart, W. 2023. Accelerated Miocene incision along the Yangtze River driven by headward drainage basin expansion. Science Advances, 9(36), eadh1636. https://doi.org/10.1126/sciadv.adh1636

Roychowdhury, M. 2019. Mahanadi valley basin structure and tectonics: In: Acharyya, S.K. (ed.) Developments in Structural Geology and Tectonics (vol 4): Tectonic Setting and Gondwana Basin Architecture in the Indian Shield. Geological Survey of India, Kolkata, pp. 95-102.

Royden, L., Perron, J.T. 2013. Solutions of the stream power equation and application to the evolution of river longitudinal profiles. Journal of Geophysical Research Earth Surface, 118(2), 497-518. https://doi.org/10.1002/jgrf.20031

Sanyal, S., Sengupta, P. (2012) Metamorphic evolution of the Chotanagpur Granite Gneiss Complex of the East India Shield: current status. Geological Society London Special Publications, 365, 117-145. https://doi.org/10.1144/SP365.7

Sarkar, A., Patel, P.P. (2009) Drainage Analysis of the Dulung Basin. In: Sharma, H.S. and Kale, V.S. (ed.) *Geomorphology In India*, Prayag Pustak Bhavan, Allahabad, pp. 133-154.

Sarkar, A., Patel, P.P. (2011) Topographic Analysis of The Dulung R. Basin. *Indian Journal of Spatial Science,* Vol. II(1), 2.

Sarkar, A., Patel, P.P. (2012) Terrain Classification of the Dulung Drainage Basin. *Indian Journal of Spatial Science*, Vol. III(1), 6.

Sarkar, A.N., 1982. Precambrian tectonic evolution of eastern India: a model of converging microplates. *Tectonophysics*, *86*(4), 363-397.

Sarkar, S.N. and Saha, A.K., 1977. The present status of the Precambrian stratigraphy, tectonics and geochronology of Singhbhum-Keonjhar-Mayurbhanj region, eastern India. Indian J. Earth Sci., S. Roy Vol., 37-65.

Schoenbohm, L. M., Whipple, K. X., Burchfiel, B. C., & Chen, L. 2004. Geomorphic constraints on surface uplift, exhumation, and plateau growth in the Red River region, Yunnan Province, China. Geological Society of America Bulletin, 116(7), 895–909. https://doi.org/10.1130/B25364.1

Schwanghart, W. and Scherler, D.: Bumps in river profiles: uncertainty assessment and smoothing using quantile regression techniques, Earth Surface Dynamics, 5, 821–839, https://doi.org/10.5194/esurf-5-821-2017, 2017.

Schwanghart, W. and Scherler, D., 2014. TopoToolbox 2–MATLAB-based software for topographic analysis and modeling in Earth surface sciences. *Earth Surface Dynamics*, *2*(1), 1-7. https://doi.org/10.5194/esurf-2-1-2014.

Schwanghart, W., Molkenthin, C. and Scherler, D., 2021. A systematic approach and software for the analysis of point patterns on river networks. *Earth Surface Processes and Landforms*, *46*(9), 1847-1862.

Scott, D.N. and Wohl, E.E., 2019. Bedrock fracture influences on geomorphic process and form across process domains and scales. *Earth Surface Processes and Landforms*, *44*(1), pp.27-45.

Sequeira, N., Bhattacharya, A. 2020. Early Neoproterozoic Deformation Kinematics in the Chottanagpur Gneiss Complex (Eastern India): Evidence from the Curvilinear Hundru Falls Shear Zone Analysis. Lithosphere 2020 (1): 8820919. https://doi.org/10.2113/2020/8820919

Shen, K., Dong, S. and Wang, Y., 2023. Active Tectonics Assessment Using Geomorphic and Drainage Indices in the Sertengshan, Hetao Basin, China. *Remote Sensing*, *15*(13), 3230. https://doi.org/10.3390/rs15133230.

Singh, R., Khan, P.K. 2021. Crustal Configuration and Seismic Stability of the Eastern Indian Shield and Adjoining Regions: Insights for Incidents of Great Earthquakes in the Nepal-Bihar-Sikkim Himalaya. Frontiers in Earth Science, 9, 586152. https://doi.org/10.3389/feart.2021.586152

Sklar, L.S., Dietrich, W.E. 2006. The role of sediment in controlling steady-state bedrock channel slope: Implications of the saltation–abrasion incision model. Geomorphology, 82, 58-83.

Slowik, M., Dezso, J., Marciniak, A., Toth, G., Kovacs, J. 2018. Evolution of river planforms downstream of dams: effect of dam construction or earlier human-induced changes? Earth Surface Processes and Landforms, 43(10), 2045-2063. https://doi.org/10.1002/esp.4371

Smith, A.G.G., Fox, M., Schwanghart, W., Carter, A. 2022. Comparing methods for calculating channel steepness index. Earth-Science Reviews, 227, 103970. https://doi.org/10.1016/j.earscirev.2022.103970

Solanki, A. and Gupta, V., 2022. Implications of geomorphometric parameters on the occurrence of landslides in the Kali Valley, Kumaun Himalaya, India. *Catena 215*, 106313. https://doi.org/10.1016/j.catena.2022.106313

Sonam, Jain, V., Fryirs, K., Brierley, G. 2022. Geomorphic characterization of seasonal river network in semi-arid western India using the River Styles Framework. Journal of Asian Earth Sciences: X, 7, 100077. https://doi.org/10.1016/j.jaesx.2021.100077

Sorrentino, A., Valente, E. and Mondillo, N., 2023. Spatial distribution of rock uplift in the Bongarà district (Peruvian Andes) and implications for the genesis of supergene ore deposits. *Geomorphology*, *439*, 108861, https://doi.org/10.1016/j.geomorph.2023.108861

Stokes, M., Mather, A.E., Belfoul, M., Faik, F., Bouzid, S., Geach, M.R., Cunha, P.P., Boulton, S.J. and Thiel, C., 2017. Controls on dryland mountain landscape development along the NW Saharan desert

margin: Insights from Quaternary river terrace sequences (Dadès River, south-central High Atlas, Morocco). *Quaternary Science Reviews*, *166*, 363-379. https://doi.org/10.1016/j.quascirev.2017.04.017.

Strahler, A.N., 1952. Hypsometric (area-altitude) analysis of erosional topography. *Geological society of America bulletin*, *63*(11), 1117-1142.

Struth, L., Garcia-Castellanos, D., Viaplana-Muzas, M., Vergés, J., 2019. Drainage network dynamics and knickpoint evolution in the Ebro and Duero basins: From endorheism to exorheism. Geomorphology 327, 554–571. https://doi.org/10.1016/j.geomorph.2018.11.033.

Subrahmanyam, V., Subhramanyam, A.S., Murty, G.P.S., Murthy, K.S.R. 2008. Morphology and tectonics of Mahanadi Basin, northeastern continental margin of India from geophysical studies. Marine Geology, 253(1-2), 63-72. https://doi.org/10.1016/j.margeo.2008.04.007

Taloor, A.K., Joshi, L.M., Kotlia, B.S., Alam, A., Kothyari, G.C., Kandregula, R.S., Singh, A.K. and Dumka, R.K., 2021. Tectonic imprints of landscape evolution in the Bhilangana and Mandakini basin, Garhwal Himalaya, India: a geospatial approach. *Quaternary International*, *575*, 21-36. https://doi.org/10.1016/j.quaint.2020.07.021.

Taloor, A.K., Sharma, R., Kothyari, G.Ch. 2023. Tectono-geomorphic and active deformation studies in the Ujh basin of Northwestern Himalaya. Quaternary Science Advances, 12, 100121. https://doi.org/10.1016/j.qsa.2023.100121

Talukdar, D., Ganguli, S.S., Ghosh, A., Sahu, B.K., Mohanty, M., Raul, A.K. 2024. Uncovering the hidden architecture of the Rengali Province, eastern Indian Shield using high-resolution aero-geophysics, ground-gravity, structure: insights towards geology and tectonics. Journal of Asian Earth Sciences. https://doi.org/10.1016/j.jseaes.2024.106416

Trevisani, S., Skrypitsyna, T.N., Florinsky, I.V. 2023. Global digital elevation models for terrain morphology analysis in mountain environments: insights on Copernicus GLO-30 and ALOS AW3D30 for a large alpine area. Environmental Earth Sciences, 82, 198. https://doi.org/10.1007/s12665-023-10882-7

Troiani, F., Galve, J.P., Piacentini, D., Della Seta, M., Guerrero, J. 2014. Spatial analysis of stream length-gradient (*SL*) index for detecting hillslope processes: A case of the Gállego River headwaters (Central Pyrenees, Spain). Geomorphology, 214, 183-197. https://doi.org/10.1016/j.geomorph.2014.02.004

Tucker, G.E. and Whipple, K.X., 2002. Topographic outcomes predicted by stream erosion models: Sensitivity analysis and intermodel comparison. *Journal of Geophysical Research: Solid Earth*, *107*(B9), pp.ETG-1. https://doi.org/10.1029/2001JB000162.

Vanik, N., Patidar, A.K., Kumar, A., A L, A., Mishra, V., 2023. Terrain analysis and hydrogeomorphic investigation of the Sita-Swarna river basin, Udupi, SW India: Insights from remote sensing methods. Quaternary Science Advances 12, 100125. https://doi.org/10.1016/j.qsa.2023.100125.

Vidya, K.M., Manoharan, A.N. and Deepchand, V., 2023. Investigating the Tectonic and Structural Controls on the Geomorphic Evolution of Shiriya River Basin, Southern India. *Journal of the Geological Society of India*, *99*(9), 1292-1304.

Wang, X., Vandenberghe, J., Huayu, L., Van Balen, R. 2017. Climatic and tectonic controls on the fluvial geomorphology of the Northeastern Tibetan Plateau (China). Journal of Geographical Sciences, 27(11), 1325-1340. https://doi.org/10.1007/s11442-017-0000-0

Wang, Y., Zhang, H., Zheng, D., von Dassow, W., Zhang, Z., Yu, J. and Pang, J., 2017. How a stationary knickpoint is sustained: New insights into the formation of the deep Yarlung Tsangpo Gorge. *Geomorphology*, *285*, 28-43. https://doi.org/10.1016/j.geomorph.2017.02.005.

Wang, Y., Zhang, H., Zheng, D., Yu, J., Pang, J. and Ma, Y., 2017. Coupling slope–area analysis, integral approach and statistic tests to steady-state bedrock river profile analysis. *Earth Surface Dynamics*, *5*(1), pp.145-160. doi:10.5194/esurf-5-145-2017

Wang, Y., Zheng, D., Zhang, H. 2022. The methods and program implementation for river longitudinal profile analysis—RiverProAnalysis, a set of open-source functions based on the Matlab platform. Science China Earth Sciences, 65, 1788-1809. https://doi.org/10.1007/s11430-021-9938-x

Wang, Y.Z., Mudd, S.M., 2021. Evidence for and against landscape transience in the Northern Qinling Mountains, China. Geomorphology 391. https://doi.org/10.1016/j.geomorph.2021.107890.

Weaver, B.L., 1990. Early Precambrian basic rocks of India. In *Early Precambrian Basic Magmatism.* 339-351. Dordrecht: Springer Netherlands.

Whipple, K.X. and Tucker, G.E., 1999. Dynamics of the stream-power river incision model: Implications for height limits of mountain ranges, landscape response timescales, and research needs. *Journal of Geophysical Research: Solid Earth*, *104*(B8), 17661-17674. https://doi.org/10.1029/1999JB900120.

Whipple, K.X., 2001. Fluvial landscape response time: How plausible is steady-state denudation?. *American Journal of Science*, *301*(4-5), 313-325.

Whipple, K.X., 2004. Bedrock rivers and the geomorphology of active orogens. *Annu. Rev. Earth Planet. Sci.*, *32*, 151-185.

Whipple, K.X., Forte, A.M., DiBiase, R.A., Gasparini, N.M. and Ouimet, W.B., 2017. Timescales of landscape response to divide migration and drainage capture: Implications for the role of divide mobility in landscape evolution. *Journal of Geophysical Research: Earth Surface*, *122*(1), 248-273. https://doi.org/10.1002/2016JF003973.

Whittaker, A.C., Cowie, P.A., Attal, M., Tucker, G.E. and Roberts, G.P., 2007. Bedrock channel adjustment to tectonic forcing: Implications for predicting river incision rates. *Geology*, *35*(2), 103-106.

Willett, S.D., McCoy, S.W., Perron, J.T., Goren, L. and Chen, C.Y., 2014. Dynamic reorganization of river basins. *Science*, *343*(6175), 1248765. https://doi.org/10.1126/science.1248765.

Willgoose, G. and Hancock, G., 1998. Revisiting the hypsometric curve as an indicator of form and process in transport-limited catchment. *Earth Surface Processes and Landforms: The Journal of the British Geomorphological Group*, *23*(7), 611-623.

Wobus, C., Whipple, K.X., Kirby, E., Snyder, N., Johnson, J., Spyropolou, K., Crosby, B. and Sheehan, D., 2006. Tectonics from topography: Procedures, promise, and pitfalls. https://doi.org/10.1130/2006.2398(04).

Yaaqoub, A. and Essaifi, A., 2023. Drainage rearrangement and landscape evolution: Insights from the Moroccan Massif Central. *Geomorphology*, *437*, 108811. https://doi.org/10.1016/j.geomorph.2023.108811.

Yang, R., Willett, S.D. and Goren, L., 2015. In situ low-relief landscape formation as a result of river network disruption. *Nature*, *520*(7548), pp.526-529.

Yang, Y., Zhou, L., Zhu, L., Liu, W. and Wang, J., 2023. Impact of upstream reservoirs on geomorphic evolution in the middle and lower reaches of the Yangtze River. *Earth Surface Processes and Landforms*, *48*(3), 582-595.

Yanites, B.J. 2018. The Dynamics of Channel Slope, Width, and Sediment in Actively Eroding Bedrock River Systems. Journal of Geophysical Research: Earth Surface, 123(7), 1504-1527. https://doi.org/10.1029/2017JF004405

Yao, W., Lyu, X., Lei, D., Wu, P. 2024. Fluvial geomorphic parameters of the Shuiluo River Catchment and their tectonic implications, SE Tibetan Plateau. Progress in Earth and Planetary Science, 11, 31. https://doi.org/10.1186/s40645-024-00636-9

Yin, J., Li, H., Xiao, K. 2023. Origin of banded iron formations: links with paleoclimate, paleoenvironment, and major geological processes. Minerals, 13(4), 547. https://doi.org/10.3390/min13040547

You, Y., Li., Z., Gao, P., Hu., T. 2022. Impacts of dams and land use changes on hydromorphology of braided channels in the Lhasa River of the Qinghai-Tibet Plateau, China. International Journal of Sediment Research, 37(2), 214-228. https://doi.org/10.1016/j.ijsrc.2021.07.003

Zaprowski, B.J., Pazzaglia, F.J., Evenson, E.B. 2005. Climatic influences on profile concavity and river incision. Journal of Geophysical Research: Earth Surface, 110, F03004. https://doi.org/10.1029/2004JF000138

Zhao, J., Li, H., Cai, X., Chen, F., Wang, L. and Yu, D., 2020. Long-term (2002–2017) impacts of Danjiangkou dam on thermal regimes of downstream Han River (China) using Landsat thermal infrared imagery. *Journal of Hydrology*, *589*, p.125135.

Zhou, L., Liu, W., Chen, X., Wang, H., Hu, X., Li, X. and Schwanghart, W., 2021. Relationship between dams, knickpoints and the longitudinal profile of the upper Indus river. *Frontiers in Earth Science*, *9*, 660996. https://doi.org/10.3389/feart.2021.660996.

Zhou, Y., Gao, Y., Shen, Q., Yan, X., Liu, X., Zhu, S., Lai, Y,. Li, Z., Lai., Z. 2022. Response of channel morphology to climate change over the past 2000 years using vertical boreholes analysis in Lancang River Headwater in Tibetan Plateau. Water, 14(10), 1593. https://doi.org/10.3390/w14101593

Figure captions

Figure 1: Location of the Brahmani River Basin in eastern India, with relief map generated from GLO-30 DEM, with 280 sub-watersheds of Brahmani River Basin based on stream ordering after Strahler (1952).

Figure 2: (a) Geomorphological map and (b) Geological map for the study area, overlain on the base DEM.

Figure 3: (a) Bilinear interpolation of average annual precipitation obtained from TRMM 2B31 v6 5 × 5 km gridded data (http://www.geog.ucsb.edu/~bodo/TRMM/), also depicting climatic classification zones according to Köppen (1931). Line diagram showing sub-basin wise precipitation and hypsometric integral. (b) Bilinear interpolation showing lineament density coupling with distribution of recent seismic activities and thermal springs with their surface temperature.

Figure 4: Morphometric parameters- Basin-mean bifurcation ratio (Rbm), Circulatory ratio (Rc), Elongation ratio (Re), Form factor (Ff), Drainage texture (Dt), Hypsometric integral (HI), Mean basin Ksn (K_{sn} $m^{0.9}$), Asymmetry factor (Af), Average annual precipitation (rain) of 280 sub-watersheds of Brahmani river basin.

Figure 5: Topographic swath profiles along the trunk channels of the Brahmani River and its primary tributaries– Sankh, South Koel and North Karo, showing structural deformations, locations of dams, and low relief landscapes.

Figure 6: (a) Lithological units overlain by Normalized steepness index (K_{sn}) values in Brahmani River basin, highlighting the types of knickpoints (lithological, tectonic-structural and anthropogenic); (b) Longitudinal profile depicting changes in SL and K_{sn} values with variations in lithological units along selected rivers.

Figure 7: Box and whisker plot showing K_{sn} values in different lithological units.

Figure 8: Correlogram of geomorphometric parameters. Positive correlations are displayed in green and negative correlations are in pink colours.

Note: A: Basin area ; Af: Asymmetry factor ; Bh: Basin relief ; Bs: Basin slope ; Cc: Compactness coefficient ; Ccm: Constant of channel maintenance ; Dd: Drainage density ; Dis: Dissection index ; Dt: Drainage texture ; Ff: Form factor ; Fs: ; Hi: Hypsometric integral; If: ; Lb: Length of Basin ; Lg: Length of overland flow ; Lu: Total length of stream segments in basin; Nu: Total number of stream segments in basin; P: Basin perimeter; Rbm: Average bifurcation ratio of basin; Rc: Circularity ratio ; Re: Elongation ratio ; Rn: Ruggedness number ; Rr: Relief ratio ; Sh: Shape factor; Ksn: Normalized steepness index; Rain: Annual rainfall

Figure 9: Chi (χ) plots for the Brahmani River and select tributaries, showing distributions and heights of knickpoints along the longitudinal profiles.

Figure 10: Lithological unit-wise knickpoint composition.

Figure 11: Chi(χ)-values of the drainage networks of the Brahmani River Basin, and possible directions of drainage divide migration in the upper catchment zone (shown in thick black arrows).

Figure 12: Paleo-relief profiles of the Sankh (S1) and South Koel (S2) tributaries of the Brahmani, reconstructed from relict upstream segments considering three main knickpoints, also highlighting the Slope-Area (S-A) profile on the log-log plot.

Figure 13: Overlays of stream segment K_{sn} values on Google Earth imagery reveals the local structural influences (dykes and other intrusive bodies) on the drainage alignment around the confluence zone of the Sankh and South Koel rivers (b and c), that join to form the Brahmani (a)

Unravelling litho-structural and tectonic influences on geomorphic and river longitudinal profile character in the Brahmani River Basin of eastern India

Highlights

- Examines tectonic and litho-structural influence on Brahmani basin's geomorphology.
- Subwatershed morphometric parameters used to discern structural/tectonic influence.
- Longitudinal river profile analysis reveals steep channel segments and knickpoints.
- Chi-plots showcase possible stream piracy zones and drainage divide migrations.
- Reconstruction of palaeo-surfaces and past river profiles shows uplift extent.